PLOS ONE

RESEARCH ARTICLE

A multi-parametric screening platform for photosynthetic trait characterization of microalgae and cyanobacteria under inorganic carbon limitation

Priyanka Pradeep Patil[1], Imre Vass[1], Sandeesha Kodru[1,2], Milán Szabó[1,3]*

1 Institute of Plant Biology, Biological Research Centre, Szeged, Hungary, **2** Biology PhD School, Faculty of Science and Informatics, University of Szeged, Szeged, Hungary, **3** Climate Change Cluster, University of Technology Sydney, Ultimo, Australia

* szabo.milan@brc.hu

Check for updates

OPEN ACCESS

Citation: Patil PP, Vass I, Kodru S, Szabó M (2020) A multi-parametric screening platform for photosynthetic trait characterization of microalgae and cyanobacteria under inorganic carbon limitation. PLoS ONE 15(7): e0236188. https://doi.org/10.1371/journal.pone.0236188

Editor: Maya Dimova Lambreva, National Research Council of Italy, ITALY

Received: April 4, 2020

Accepted: June 30, 2020

Published: July 23, 2020

Copyright: © 2020 Patil et al. This is an open access article distributed under the terms of the Creative Commons Attribution License, which permits unrestricted use, distribution, and reproduction in any medium, provided the original author and source are credited.

Data Availability Statement: All relevant data are within the paper and its Supporting Information files.

Funding: This work was supported by the grants of M.S. received from the Hungarian Academy of Sciences, MTA Premium Postdoctoral Research Program, Grant number PREMIUM-2017-38, https://mta.hu/english/mta-premium-postdoctoral-research-program and from the National Research, Development and Innovation Office, Grant number NKFIH FK 128977, https://nkfih.gov.hu/about-the-

Abstract

Microalgae and cyanobacteria are considered as important model organisms to investigate the biology of photosynthesis; moreover, they are valuable sources of biomolecules for several biotechnological applications. Understanding the species-specific traits of photosynthetic electron transport is extremely important, because it contributes to the regulation of ATP/NADPH ratio, which has direct/indirect links to carbon fixation and other metabolic pathways and thus overall growth and biomass production. In the present work, a cuvette-based setup is developed, in which a combination of measurements of dissolved oxygen, pH, chlorophyll fluorescence and NADPH kinetics can be performed without disturbing the physiological status of the sample. The suitability of the system is demonstrated using a model cyanobacterium *Synechocystis* sp. PCC6803, as well as biofuel-candidate microalgae species, such as *Chlorella sorokiniana*, *Dunaliella salina* and *Nannochloropsis limnetica* undergoing inorganic carbon (Ci) limitation. Inorganic carbon limitation, induced by photosynthetic Ci uptake under continuous illumination, caused a decrease in the effective quantum yield of PSII (Y(II)) and loss of oxygen-evolving capacity in all species investigated here; these effects were largely recovered by the addition of $NaHCO_3$. Detailed analysis of the dark-light and light-dark transitions of NADPH production/uptake and changes in chlorophyll fluorescence kinetics revealed species- and condition-specific responses. These responses indicate that the impact of decreased Calvin-Benson cycle activity on photosynthetic electron transport pathways involving several sections of the electron transport chain (such as electron transfer via the Q_A-Q_B-plastoquinone pool, the redox state of the plastoquinone pool) can be analyzed with high sensitivity in a comparative manner. Therefore, the integrated system presented here can be applied for screening for specific traits in several significant species at different stages of inorganic carbon limitation, a condition that strongly impacts primary productivity.

office. The funders had no role in study design, data collection and analysis, decision to publish, or preparation of the manuscript.

Competing interests: The authors have declared that no competing interests exist.

Introduction

Microalgae are phototrophic organisms that play an essential role in the biogeochemical cycling of macro and microelements and are thus key components of freshwater and marine ecosystems. Besides their role in the biosphere, microalgae are also valuable sources of various compounds that have a great importance for human consumption, such as pharmaceuticals, nutraceuticals, food supplements etc. However, in order to efficiently utilize microalgae, it is essential to understand their physiology, life cycle and stress tolerance mechanisms in detail. Microalgae, as other oxygenic phototrophs, are often exposed to fluctuating environmental conditions, which can cause imbalances in metabolic reactions that ultimately affect growth and thus biomass production. The light reactions of photosynthesis, performed by several components of the photosynthetic electron transport chain, including Photosystem II (PSII), Cytochrome b_6/f, Plastocyanin, Photosystem I (PSI), together with the subsequent carbon fixation processes provide rapid regulatory mechanisms that can fine-tune the energetic balance to mitigate the detrimental effects of highly variable stress conditions. Linear electron transport originating from the oxidation of water molecules produces ATP and NADPH, which are utilized primarily in the Calvin-Benson cycle. ATP and NADPH are produced in a ratio that is often insufficient for CO_2 fixation [1]. Various stress factors can modify the ATP and NADPH generation pathways and thus the ATP/NADPH ratio, potentially causing imbalances in the cellular energy stocks. Stress conditions prime metabolism for elevated ATP demand, which can be provided by alternative electron transport mechanisms (reviewed e.g. in [2]). Cyclic electron flow around PSI (CEF) is exclusively involved in ATP synthesis without the accumulation of NADPH. Briefly, CEF involves transferring electrons from PSI to the PQ pool, mediated by the NAD(P)H PQ oxidoreductase pathway, namely the type 1 NADH dehydrogenase (NDH-1) or the type 2 NADPH dehydrogenase (NDH-2), or by the Proton Gradient Regulation/PGR5-Like Photosynthetic Phenotype 1 (PGR5/PGRL1) pathway (reviewed e.g. in [3]). This cyclic electron transfer mechanism is coupled with proton translocation from the stroma to the lumen during the Q-cycle [4], and the translocated protons are utilized by ATP synthase to produce ATP without the net synthesis of NADPH.

Inorganic carbon (Ci) in the form of bicarbonate (HCO_3^-) and/or carbon dioxide (CO_2) is the most important and essential macronutrient for the growth of organisms performing oxygenic photosynthesis. Although inorganic carbon is crucial to sustain photosynthetic carbohydrate synthesis, aquatic photosynthetic organisms are often exposed to randomly fluctuating Ci availability or sustained Ci limitation that may strongly impact primary productivity and growth. To overcome Ci limitation, photosynthetic organisms operate carbon concentrating mechanisms (CCM) that play an important role in the physiological gas-exchange characteristics by increasing the concentration of CO_2 at the active site of ribulose-1,5-bisphosphate carboxylase oxygenase (Rubisco) [5–8].

In previous works the activation of alternative electron transport mechanisms including CEF was characterized in cyanobacteria using various non-invasive biophysical methods. Variable chlorophyll fluorescence is a frequently applied tool to monitor the operating efficiency of PSII (e.g. [9, 10]), as chlorophyll fluorescence is relatively easily measured in standard cuvette systems as well as in photobioreactors, even in large scale algal cultivation facilities. The influence of inorganic carbon content on photosynthetic performance can be sensitively monitored by the Chlorophyll (Chl) fluorescence induction technique in green algae [11, 12] as well as in cyanobacteria [13, 14]. Advanced Chl fluorescence techniques such as post-illumination rise in chlorophyll fluorescence and flash-induced fluorescence decay kinetics [15] can also reveal the electron transfer steps between the Q_A, Q_B and the PQ pool. In addition, a wave phenomenon observed in fluorescence decay was found to be particularly useful to resolve specific

redox kinetics that reveal the operation of the PQ pool and electron donations towards PSI during CEF in cyanobacteria [15] and green algae [16]. Combination of Chl fluorescence with P700 kinetics, NADPH fluorescence and/or transient measurements of carotenoid bandshifts (electrochromic absorbance changes) have been previously applied to monitor the balance and shifts between LEF and CEF mechanisms under altered Ci conditions [13, 14, 17–19]. A thin-layer microcell capable of measuring flash O_2 yields and chlorophyll fluorescence by fast repetition rate (FRR) fluorometry allowed the characterization of linear and cyclic electron flow within PSII in several microalgae and cyanobacteria [20] and the analysis of PSII binding sites of HCO_3^- with different affinities under reversible inorganic carbon limitation [21].

The responses of photosynthetic electron transport to Ci limitation have been characterized in popular model species and mutants of cyanobacteria, e.g. *Synechocystis* PCC 6803 and green algae such as *Chlamydomonas reinhardtii* [6, 13, 17]. A particularly important and extensively characterized mutant of *Synechocystis* PCC 6803 is the ndhB-deficient M55 mutant, which lacks all the type 1 NADPH-dehydrogenase (NDH-1) complexes [22], and is therefore unable to perform CEF and CCM. The M55 has a high-CO_2-requiring phenotype, its photosynthetic activity remains low, and the NADP pool is highly reduced under ambient CO_2-concentrations [22–24].

The inherent regulation of photosynthesis and the plasticity of the photosynthetic electron transport chain under variable growth and environmental conditions and abiotic stress factors remains largely uncharacterized in several microalgae species that have high relevance in biotechnological applications and biofuel industries, such as *Chlorella sorokiniana*, *Dunaliella salina and Nannochloropsis limnetica*. The green alga *Chlorella sorokiniana* is considered as a stress-resilient species, and due to its ability to maintain high growth rates under stress it is applied in several industrial processes such as wastewater treatment (e.g. [25]) and elevated CO_2 sequestration which enhances lipid production [26]. The species *Dunaliella salina*, a highly salt-tolerant green alga is applied for commercial scale β-carotene production in pharmaceutical and nutraceutical industries (recently reviewed in [27]). Furthermore, this species is also an important model organism for studying photoacclimation capabilities to enhance biomass productivity (e.g. [28]).

Nannochloropsis limnetica (Eustigmatophyceae) is a freshwater alga, whose total fatty acid content can be very high, even double of the fatty acid content of other marine *Nannochloropsis* species [29]. Despite the high relevance of these species in industrial applications, the dynamic regulation of their photosynthetic responses, e.g. under transient Ci limitation has scarcely been characterized.

Precisely designed and operated photobioreactor systems with multiple sensors of physico-chemical parameters (dissolved oxygen, pH, optical density) and gas control allowed real time monitoring of the physiological changes and net photosynthesis under Ci limitation [30–33]. However, an integrated analysis system, where the physico-chemical parameters of algae suspensions can be measured along with photosynthetic efficiency parameters and the kinetics of photosynthetic electron transport in a simple cuvette-based platform has not been established and utilized for screening for photosynthetic markers in microalgae. A standardized, cuvette-based platform that allows monitoring dissolved O_2 and pH along with non-invasive measurements of advanced Chl fluorescence and NADPH fluorescence kinetics would allow screening for photosynthetic traits of uncharacterized species, under various stages of Ci limitation and recovery.

Therefore the aims of the present work were (i) to establish an integrated cuvette system, where several parameters (O_2 evolution/uptake, pH) and photosynthetic quantum efficiency and kinetics of photosynthetic electron transport can be simultaneously recorded and monitored, in time-resolved manner under well-defined environmental conditions, and (ii) to comprehensively and comparatively monitor and assess the photo-physiological and

photosynthetic behavior of *Synechocystis* sp. *PCC6803 WT* (grown with and without CO_2), the M55 mutant of *Synechocystis* sp. *PCC6803*, *Chlorella sorokiniana*, *Dunaliella salina and Nannochloropsis limnetica* under inorganic carbon limitation and during recovery from inorganic carbon limitation stress. This integrated approach would allow to investigate photosynthetic efficiency and operation of photosynthetic electron transport pathways in biofuel-candidate microalgae undergoing inorganic carbon limitation, a particularly relevant stress condition that affects photosynthetic performance and primary productivity in short timescales.

Materials and methods

Culture conditions

Synechocystis sp. PCC 6803 WT (wild type) cells were grown in BG-11 medium on a rotary shaker under continuous illumination of 40 μmol photons m^{-2} s^{-1} photon flux density white light at 30˚C, supplied by 3% CO_2 or ambient CO_2 (where 'ambient' refers to approx. 410 ppm atmospheric CO_2 concentration). The M55 mutant (ΔndhB), deficient in type I NADPH dehydrogenase complex, NDH-1 [22] of *Synechocystis* was grown under the same conditions as the WT (in 3% CO_2) in BG-11 medium supplemented with kanamycin (20 μg mL^{-1}).

Chlorella sorokiniana (Trebouxiophyceae) and *Nannochloropsis limnetica* (Eustigmatophyceae) were grown in 500 mL Erlenmeyer flasks with 200 mL culture volume in BG-11 medium with the light intensity of 56 μmol photons m^{-2} s^{-1} (white LED light), 12 h: 12 h day: night diurnal cycle with continuous shaking at 120 rpm, at a constant temperature of 24˚C.

Dunaliella salina was grown under the same conditions as described above, but in f/2 medium (prepared with artificial seawater) supplemented with 30 gL^{-1} NaCl and no shaking.

For measurements the cells were harvested in the early exponential growth phase, centrifuged at 6,500 g for 5 min at 24˚C and were resuspended in fresh medium to achieve the Chl *a* content of 5 μg mL^{-1}.

Measurement of chlorophyll content

For eukaryotic microalgae chlorophyll was determined using acetone and DMSO (1:1). The samples were centrifuged at 16,000 g for 8 min. The supernatant was discarded and 1 mL of a 1:1 mixture of 90% acetone and 90% DMSO was added to the pellet, then incubated on ice for 5 min, vortexed and centrifuged at 16,000 g for 7 min. The supernatant containing the extracted pigments was transferred to a glass cuvette with 1 cm path length for measurement. The absorbance spectrum was measured with a UV-visible spectrophotometer (UV-1601, Shimadzu corporation, Japan) at A_{663} and A_{645} nm for determining the chlorophyll *a* content, according to [34, 35] (see also S1 Table). Eq 1 was used for calculating chlorophyll *a* content for microalgae.

$$\text{Chl } a\ (\mu\text{g mL}^{-1}) = 11.75{*}A_{663} - 2.35{*}A_{645} \quad (1)$$

For cyanobacteria, the chlorophyll *a* content was determined by 100% methanol extraction. Eq 2 was used to calculate chlorophyll *a* content for *Synechocystis* sp.

$$\text{Chl } a\ (\mu\text{g mL}^{-1}) = 16.5{*}A_{665.5} - 8.3{*}A_{650.5} \quad (2)$$

Experimental setup

A cuvette-based sample holder (Optical Unit ED-101US/MD, Heinz Walz GmbH, Effeltrich, Germany) attached to a DUAL-PAM-100 chlorophyll fluorometer (Heinz Walz GmbH, Effeltrich, Germany) was used for monitoring the physiological response of microalgae. A quartz cuvette with 1 cm path length (Hellma GmbH, Germany) was used with a custom-designed

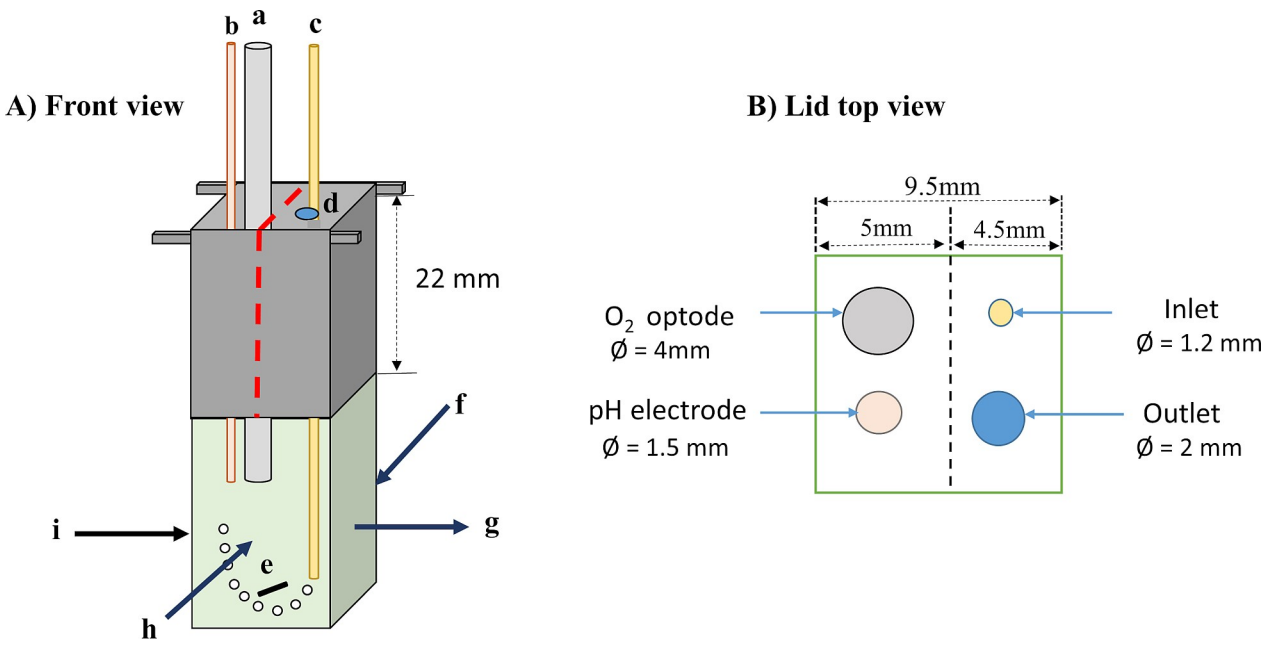

Fig 1. Cuvette-based setup with custom-designed lid including (a) O_2 optode, (b) pH electrode, (c) Inlet (air/gas bubbling), (d) Outlet, (e) Magnetic stirrer, (f) NADPH emitter, (g) NADPH detector, (h) Chlorophyll fluorescence detector, (i) Fiber optic white light source.

https://doi.org/10.1371/journal.pone.0236188.g001

lid, in which various probes were fixed in the following configuration (as shown in Fig 1): (a) a 4 mm outside diameter O_2 optode (Fibox 3, Presens GmbH, Aachen, Germany) to measure the dissolved oxygen content of the sample, (b) a 1.5 mm pH electrode (Microelectrode Inc., USA) to log the pH change, (c) a 1.2 mm inlet pipe to provide air bubbling controlled via a 18-gauge blunt tip syringe needle to avoid the buildup of excess oxygen concentration that may cause oxygen toxicity in the chamber, and (d) an outlet hole for gas exchange and pressure release.

The lid was designed in two parts: half of the lid could be easily opened and closed when needed during the experiment without disturbing the O_2 optode and the pH electrode, which can stay stable together with the other half of the lid. The temperature was maintained at 24˚C for eukaryotic microalgae and 30˚C for cyanobacteria in a temperature-controlled block (ED-101US/T Heinz Walz GmbH, Effeltrich, Germany) fixed on the Optical Unit ED-101US/MD, by using a water circulation heater chiller (Pharmacia Biotech GmbH MultiTemp III, Germany). The cuvette was closed for the duration of the O_2 evolution measurement, and opened after the measurement to allow gas exchange and to avoid the buildup of excess levels of dissolved oxygen that may cause oxygen toxicity (according to [12]). The culture was continuously stirred with a small magnetic stirrer bar. The sample was illuminated with white actinic light provided by a fiber optic light source from one side of the cuvette (Schott KL 1500, Schott AG, Germany). For NADPH measurements the Dual NADPH/9AA module was used (see below), with the emitter (Dual-ENADPH) and detector (Dual-DNAPH) units placed at right angle position to avoid the measuring light reaching the photomultiplier and reducing the level of artificial background signals. Chlorophyll fluorescence was recorded with a Dual-DB/DR unit, assembled to a right angle position to the Dual-DNADPH detector (Fig 1). Flash-induced fluorescence decay kinetics and OJIP transient curves were measured using a double-modulation PSI fluorometer (see below) that was not directly integrated into the Dual-PAM cuvette unit. The PSI-FL3000 fluorometer was equipped with a fixed measuring head (the so-

called super-head, containing the cuvette holder and the emitter detector unit), therefore the cuvette was transferred from the Dual-PAM holder into the PSI super-head.

Experimental procedure

The photophysiological response of microalgae was investigated by using variable chlorophyll fluorescence via pulse amplitude modulation (PAM) chlorophyll fluorometry, O_2 evolution and pH measurements. 2 mL working volume was loaded in the 1-cm rectangular quartz cuvette with 5 μg mL^{-1} Chl *a* suspended in fresh medium for the measurement. The cuvette was covered with a customized lid ensuring that the sample was closed, or open to gas exchange with ambient air, depending on the applied experimental conditions. The dissolved oxygen concentration was logged continuously, measured at a sampling interval of every 1 s by the manufacturer's software (OxyView—PST3-V5.32 02/2004, PreSens GmbH, Germany) via USB connection. The O_2 sensor was calibrated with two points, i.e. air-saturated water 'Cal 100' (100% air saturation) and anoxic water 'Cal 0' (1 g of Na_2SO_3 in 100 ml distilled water) before the measurement. The oxygen evolution/uptake rate was determined from the slope of the linear fitting of the original traces and expressed in μmol O_2 [mg Chl *a*]$^{-1}$ h^{-1} units. In certain experiments, changes in O_2 evolution/uptake dynamics are displayed as a rate, given by the first derivative of the dissolved oxygen traces. pH data were logged every 5 min via the manufacturer's data logging software (Orion Star A300, Thermo Scientific Inc., USA). Effective quantum yield, oxygen concentration and pH were recorded starting from the 0 min time point. In the first 20–30 min the sample was kept in the dark with a weak measuring light on to determine the minimum fluorescence (denoted as F_0 in the dark-adapted state or F_s in the light-adapted state). A 600 ms saturation light pulse (LED with peak emission at 635 nm, PPFD 10,000 μmol photons m^{-2} s^{-1}) was applied every 5 min for the determination of maximum fluorescence (denoted as F_m in the dark-adapted state or F_m' in the light-adapted state). The effective quantum yield of photochemical energy conversion in PSII in the light-adapted state was calculated as $Y(II) = (F_m' - F_s)/F_m'$ or in analogy, the expression $F_v/F_m = (F_m - F_0)/F_m$ was applied to determine the maximum quantum efficiency of PSII in the dark-adapted state [36]. After a dark period of approx. 25 min the sample was illuminated with actinic white light with the same irradiance that was applied as a growth light, to induce inorganic carbon uptake, until cells achieved a Ci-limited state. Each species required different time periods to reach the Ci-depleted phase, therefore the AL was provided for specified time periods as indicated at the individual experiments (see below in Fig 2 and S1–S6 Figs). To restore the photosynthetic activity of the cells, 10 mM $NaHCO_3$ was added at the fully Ci-depleted stage. At defined time points, the NADPH and Chl fluorescence measurements were performed as specified below. The flash-induced fluorescence decay kinetics and OJIP transient curves were measured by transferring the cuvette to the PSI measuring head without removing the lid or the sensors, therefore neither the physiological and physico-chemical conditions of the cell suspensions were disturbed, nor the Ci content of the cells and the geometry of the cuvette setup were changed throughout the whole process/experiment.

Simultaneous measurement of NADPH and chlorophyll fluorescence

NADPH and chlorophyll fluorescence were simultaneously measured in a Dual-PAM-100 chlorophyll fluorometer (Heinz Walz, Effeltrich, Germany) at 24˚C for green algae and 30˚C for cyanobacteria. At a specific time point representing either the Ci-replete or -depleted stage (defined as T points, see Results and Discussion), cells were dark-adapted for 3 min. A slow induction measuring protocol was initiated and the NADPH/Chl fluorescence signals were recorded for 30 s in the dark to establish a baseline, then the actinic red light (635 nm peak intensity) at ~56 μmol photons m^{-2} s^{-1} (or near the growth light intensity) was switched on to

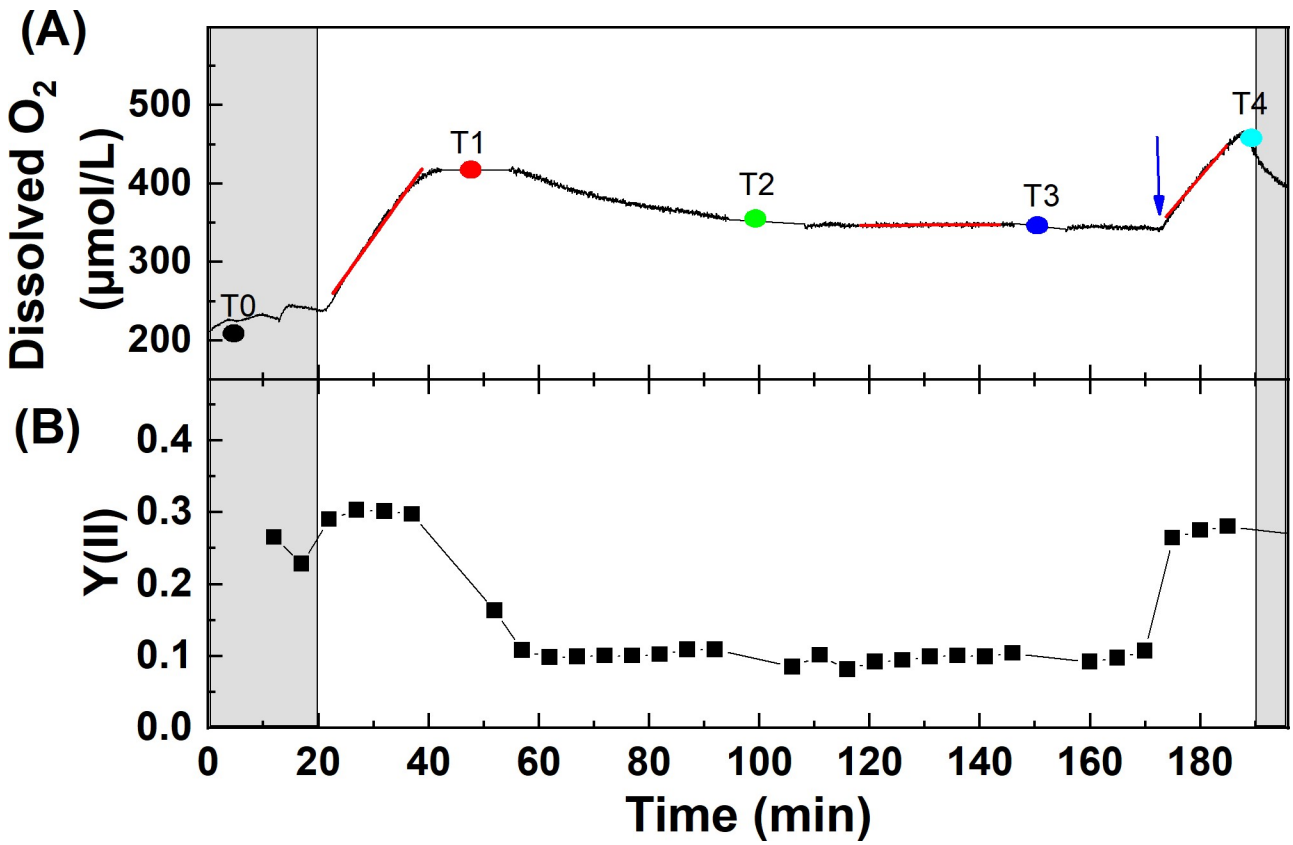

Fig 2. Representative graph of the physiological response of *Synechocystis* sp. PCC6803 WT during the course of Ci limitation. The cells were washed and resuspended in fresh HEPES buffered BG11 medium. Simultaneous measurements of (A) Oxygen evolution and (B) Effective quantum yield of PSII (Y(II)) were performed. Y(II) was measured every 5 min. The cells were kept in the dark for 20 min (grey shade region), then illuminated with actinic white light at 56 µmol photons m^{-2} s^{-1}. The dots in panel A represent the defined measuring time points of chlorophyll and NADPH fluorescence kinetics at: T0 (control) in the dark, T1—initial Ci-replete phase in the light, T2—early phase of Ci depletion, T3—prolonged Ci-depleted phase, T4—Ci recovery phase in the light (arrow indicates the addition of 10 mM $NaHCO_3$). The red lines represent the phases to determine O_2 evolution/uptake rates.

https://doi.org/10.1371/journal.pone.0236188.g002

record light-induced NADPH/Chl fluorescence change for 180 s, and subsequently the NADPH/Chl fluorescence change from light-to-dark was monitored up to 300 s.

NADPH fluorescence was measured using the NADPH/9-AA module of a Dual-PAM-100 instrument (Heinz Walz, Effeltrich, Germany; [37–39]). The NADPH/9-AA module consists of an emitter unit (DUAL-ENADPH) and a detector unit (DUAL-DNADPH). NADPH fluorescence was excited by UV-A (365 nm) from the DUAL-ENADPH unit and detected by a blue-sensitive photomultiplier with a filter transmitting light between 420 and 580 nm in the DUAL-DNADPH unit. The measuring light intensity was set to 20, the measuring light frequency in the absence and presence of red AL was set at 200 and 5,000 Hz, respectively. Chl fluorescence was detected with a Dual-DB/DR unit (see Fig 1 for the topological arrangement of the measuring setup and refer to [38] for the technical details of the emitter-detector units).

Measurement of flash-induced chlorophyll fluorescence decay and OJIP transients

Flash-induced chlorophyll fluorescence decay was measured in the same cuvette that was used for measuring simultaneous Chl-NADPH fluorescence using a double-modulation

fluorometer (FL-3000, Photon System Instruments, Drásov, Czech Republic). The measuring unit was controlled by the manufacturer's software (FluorWin, Photon System Instruments, Drásov, Czech Republic). The timing and duration of the flashes were defined in the FluorWin experimental protocol and executed by a microprocessor in the control unit of the fluorometer. After 4 measuring flashes (8 μs, 620 nm) to determine minimum fluorescence in the dark, a single turnover saturating actinic flash (30 μs, 639 nm) was applied, which transfers an electron from the water oxidizing complex to Q_A, resulting in a prompt increase in fluorescence as a result of formation of Q_A^- [15]. The fluorescence decay resulting from reoxidation of Q_A^- was measured by applying measuring flashes in the time range from 150 μs to 100 s on a logarithmic time scale. OJIP transient curves were recorded by applying continuous illumination with strong actinic light for 3 s (639 nm peak wavelength, PPFD ~3,000 μmol photons m^{-2} s^{-1}).

Data analysis

Graphs were plotted and analyzed using OriginPro 2018 software. To test statistical differences between the Ci replete, depleted and recovery, paired-sample t-test was applied using the OriginPro 2018 software. The flash-induced fluorescence decay curves and the OJIP transients were double normalized; minimal fluorescence F_0 was set to 0 and maximal fluorescence was set to 1.

Results and discussion

Continuous monitoring of physiological changes under Ci limitation

In a typical experiment in WT *Synechocystis* cells (Fig 2), after recording the respiratory oxygen uptake in the dark, a significant increase in dissolved oxygen content was observed in the presence of actinic light, indicating active oxygen evolution by photosynthesis. Upon prolonged illumination, the rate of oxygen evolution decreased as cells gradually entered a Ci-depleted stage. After about 20 min of illumination, oxygen evolving capacity was reversibly lost as *Synechocystis* cells became Ci-depleted, and the dissolved oxygen level slightly decreased as a result of oxygen uptake by the cells, potentially due to the activation of oxygen uptake mechanisms (e.g. [40]). The effective quantum yield of PSII (Y(II)) in the light-adapted state (or F_v/F_m, maximum quantum yield of PSII in the dark-adapted state) increased upon illumination (during dark to light transition), probably due to state 2 to state 1 transition [41], then after attaining a plateau for 15–20 min, Y(II) decreased gradually during the course of prolonged illumination and attained a steady-state level after ~25 min of illumination (Fig 2). After addition of $NaHCO_3$, Y(II) and oxygen evolution recovered to 80–90% of the values observed at the beginning of the illumination (initially carbon-replete stage), indicating that the decrease in oxygen evolution capacity and effective quantum yield occurred as a result of Ci depletion during illumination (the irradiance was unchanged during $NaHCO_3$ addition). The results of continuous monitoring of dissolved O_2, Y(II), and pH for the entire experiments for all species are shown in the Supplementary material (S1–S6 Figs). The pH during the experiments remained unchanged in the cultures grown and suspended in BG-11 (pH = 7.5–7.7, S1–S5 Figs). However, in the case of *D. salina* cultivated in f/2 medium, the pH showed a progressive increase from pH = 7.7 to a plateau of 9.2 (S6 Fig), as the cells entered the Ci-limited stage (for the relationship between extracellular pH and Ci content in algae cultivated in an artificial seawater based medium, refer to [18, 32]). The simultaneously recorded oxygen and chlorophyll fluorescence data in the integrated cuvette system allows displaying the dynamic changes in photosynthetic processes in various stages of Ci limitation/recovery. Dynamic changes in oxygen evolving capacity (i.e. the rate, given by the first derivative of changes in dissolved oxygen level) displayed along with PSII electron transfer rate (ETR) showed a good

correlation in all species. However, in some cases at the beginning of the experiment, especially in microalgae, oxygen evolution rate was found to be relatively low as compared to Y(II), which is possibly due to the operation of active oxygen uptake mechanisms (S7 Fig shows the original plots for all species investigated here).

The reversible loss of O_2 evolution capacity and decrease in PSII quantum yield under bicarbonate depletion are in agreement with earlier findings that were obtained by simultaneous O_2 yield and variable Chl fluorescence assays. In Ref. [42] it was found that addition of 10 mM $NaHCO_3$ to Ci-depleted *Synechocystis* cells caused a 2-fold stimulation of oxygen evolution. In a mutant that is deficient of the arginine binding site of the CP43 protein (R357S), the stimulating effect of $NaHCO_3$ addition on O_2 evolution was much less expressed or completely missing. Bicarbonate has an important regulatory role in both the donor and acceptor sides of PSII (reviewed e.g. in [43]). On the donor side, bicarbonate was found to play a role in photo-induced assembly of the manganese cluster of the water-oxidizing complex, stabilization of PSII and protection of PSII against photoinhibition and thermoinactivation (reviewed in [44]). On the acceptor side bicarbonate is coordinated to the non-heme iron located between Q_A and Q_B [45] and therefore plays an important role in the regulation of electron transport from Q_A^- to Q_B, the protonation of Q_B^{2-} and the exchange of Q_BH_2 with the PQ pool (studied extensively by Govindjee and colleagues, reviewed e.g. in [46, 47]).

Comparative analysis of effective quantum yield of PSII under Ci limitation

Effective quantum yield of PSII (Y(II)) in the initial Ci replete stage (T1 phase) showed specific differences in *Synechocystis* sp. PCC6803; cultures grown in the presence of 3% CO_2 and at ambient CO_2 exhibited Y(II) = 0.39±0.1 and Y(II) = 0.29±0.01, respectively, whereas the M55 mutant showed Y(II) = 0.05±0.02. Under prolonged Ci-limited stage (T3 phase), Y(II) significantly dropped to 0.11±0.04 and to 0.15±0.05 in cells grown at 3% CO_2 and at ambient CO_2, respectively (when compared to Ci-replete, $p<0.05$, Fig 3), while in the M55 mutant Y(II) remained essentially unchanged (Y(II) = 0.05±0.03). Upon addition of $NaHCO_3$, Y(II) recovered to 0.35±0.07 and to 0.29±0.04 in cultures grown at 3% CO_2 and at ambient CO_2, respectively, and to 0.36±0.04 in the M55 mutant. This indicates that the M55 cells were probably Ci-limited from the beginning (even though they were cultivated at 3% CO_2), and only after the addition of 10 mM $NaHCO_3$ did they regain maximal PSII quantum efficiency. This was not due to lack of functional PSII reaction centres, because dark-adapted F_v/F_m was found to be 0.45±0.02 in the M55 mutant (S3 Fig).

In the species *C. sorokiniana*, *D. salina* and *N. limnetica*, the behavior of Y(II) under Ci depletion and recovery was similar. With the continuous illumination of actinic white light (for approx. 3.5h), Y(II) significantly decreased, and upon addition of $NaHCO_3$ Y(II) recovered nearly completely in all three species. The dynamics of the chlorophyll fluorescence parameters (original chlorophyll fluorescence traces are shown in S8 Fig) indicates that minimal steady-state fluorescence (F_s) in *Synechocystis* grown at 3% CO_2 increases during actinic illumination and remains at a high level during the onset of Ci limitation, and after addition of $NaHCO_3$ it recovers to the initial Ci-replete stage (S8A Fig). However, *Synechocystis* grown at ambient CO_2 exhibited only a small increase in F_s under actinic illumination (S8B Fig), suggesting that the PQ pool remained at a more oxidized state during the Ci limitation experiment in *Synechocystis* cells grown at ambient CO_2 level as compared to the 3% CO_2 growth condition. This effect is probably due to the operation of an alternative electron flow, such as photorespiration [48] (or more likely due to the flavodiiron-mediated O_2 consumption [49]). M55 showed a rapid increase in steady-state fluorescence (F_s) (S8C Fig) and a decrease in F_m' within

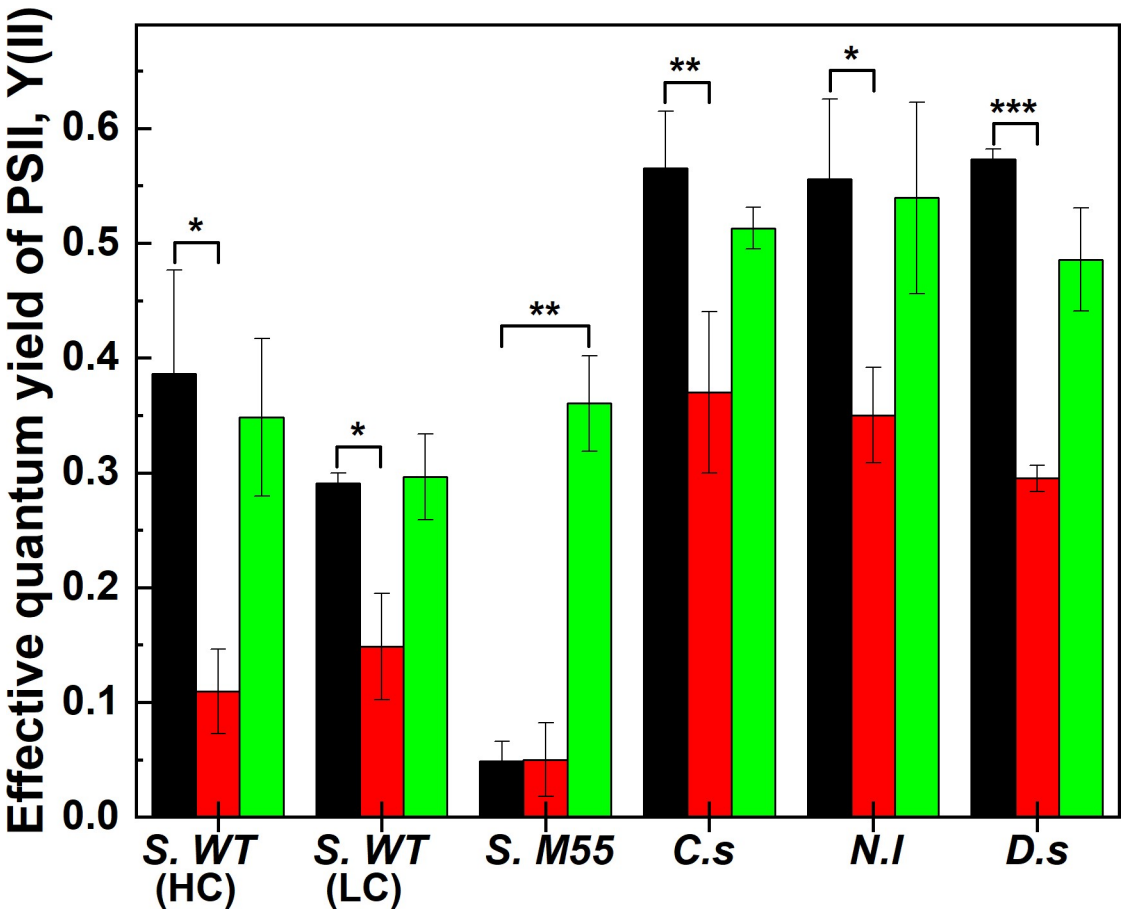

Fig 3. Effective quantum yield of PSII in Ci-replete (black), -depleted (red) and recovery (green) stages. The values are presented as a mean ± SD (n = 3) indicated by error bars. The asterisks mark significant difference between the indicated states (single asterisks (*): $p<0.05$, double asterisks (**): $p<0.01$, triple asterisks (***): $p<0.001$). Abbreviations: S. WT (HC) (*Synechocystis* sp. PCC6803 WT High CO_2 grown), S. WT (LC) (*Synechocystis* sp. PCC6803 WT Low (ambient) CO_2 grown), S. M55 (*Synechocystis* M55 mutant), C.s (*Chlorella sorokiniana*), N.l (*Nannochloropsis limnetica*), D.s (*Dunaliella salina*).

https://doi.org/10.1371/journal.pone.0236188.g003

5 min of actinic light illumination that corresponds to the immediate drop in Y(II) in the light (S3 Fig). F_s remained at high level and F_m' remained smaller during the onset of Ci limitation, which was recovered after the addition of $NaHCO_3$ to the initial Ci-replete stage. *C. sorokiniana* (S8D Fig) exhibited a moderate increase in F_s after 60–70 min of actinic illumination, which coincided with the cessation of oxygen evolution and drop in Y(II). Prolonged illumination caused a decrease in F_m', most probably due to the activation of non-photochemical quenching processes as a potential energy dissipating mechanism under Ci limitation. *N. limnetica* (S8E Fig) also exhibited an increase in F_s under prolonged illumination, however F_m' remained relatively constant under Ci limitation. *D. salina* (S8F Fig) exhibited a continuous and progressive decrease in both F_s and F_m' probably as a result of activation of non-photochemical quenching mechanisms under Ci limitation.

Comparative analysis of photosynthetic oxygen evolution rates under Ci limitation

During the course of prolonged illumination significant loss in the O_2 evolving capacity was observed in all species in Ci-depleted state (Fig 4). Oxygen evolution in Ci-replete state was

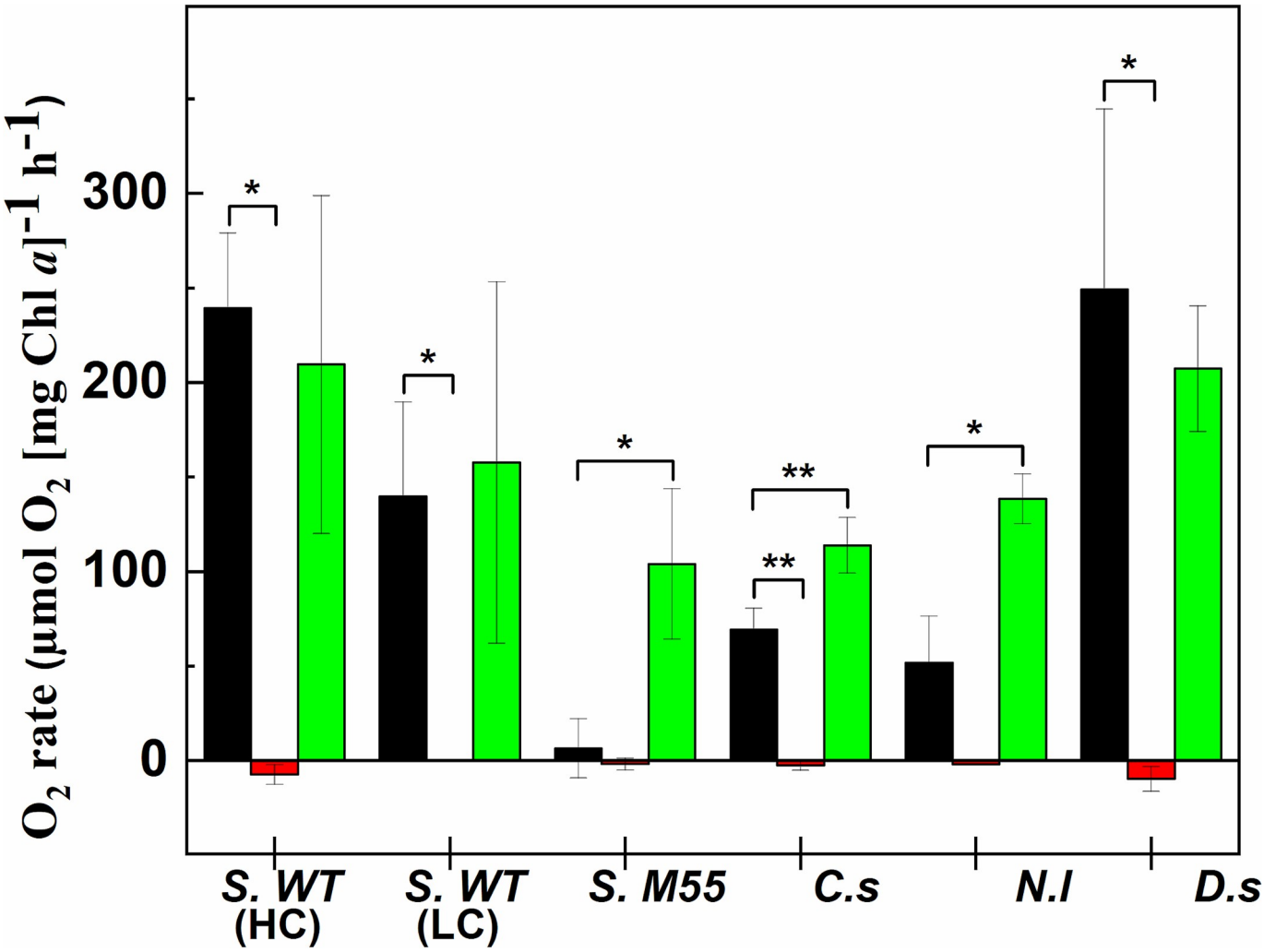

Fig 4. Rate of O_2 evolution or uptake measured in Ci-replete (black), -depleted (red) and recovery (green) stages. Rate of O_2 was calculated from the linear slope of dissolved O_2 obtained during Ci limitation (red lines in Fig 2). Values are presented as a mean ± SD (n = 3) indicated by error bars. The asterisks mark significant difference between the indicated states (single asterisks (*): $p<0.05$, double asterisks (**): $p<0.01$, triple asterisks (***): $p<0.001$). Abbreviations: S. WT (HC) (*Synechocystis* sp. PCC6803 WT High CO_2 grown), S. WT (LC) (*Synechocystis* sp. PCC6803 WT Low (ambient) CO_2 grown), S. M55 (*Synechocystis* M55 mutant), C.s (*Chlorella sorokiniana*), N.l (*Nannochloropsis limnetica*), D.s (*Dunaliella salina*).

https://doi.org/10.1371/journal.pone.0236188.g004

found to be 239.3±40 μmol O_2 (mg Chl *a*)$^{-1}$ h^{-1} (all O_2 rate values are expressed in the same units) in *Synechocystis WT PCC6803* 3% CO_2 grown samples, 139.7±50 in *Synechocystis WT PCC6803* grown at ambient CO_2 and 6.55±15.6 in the M55 mutant. Oxygen evolution rate was 69.4±11.25 in *Chlorella sorokiniana*, 51.9±24.6 in *Nannochloropsis limnetica* and 249.4±58.1 in *Dunaliella salina*. Under Ci-limited conditions, O_2 evolution capacity was essentially lost and negative rates could be observed, indicating that the O_2 uptake rate exceeded the rate of O_2 evolution under Ci limitation. The O_2 evolution capacity was significantly regained in the recovery phase (after addition of $NaHCO_3$) in *Synechocystis* grown both at 3% and ambient CO_2. In the case of the M55 mutant, O_2 evolution after $NaHCO_3$ addition was significantly higher, 104.07±39.7 ($p<0.05$) as compared to the initial 'Ci-replete' stage, indicating that the M55 mutant was heavily Ci-limited during growth and at the beginning of the experiment. In microalgae, O_2 evolution recovered to 113.9±14.7 ($p<0.01$) in *C. sorokiniana*, to 138.56±13.18 ($p<0.05$) in *N. limnetica*, and to 207.4±33.3 in *D. salina*.

NADPH fluorescence kinetics under Ci limitation

NADPH fluorescence kinetics is a versatile probe to investigate several photosynthetic processes downstream of PSI, the operation of ferredoxin $NADP^+$ oxidoreductase (FNR), activation and limitations of the Calvin-Benson cycle. This method has been proven especially useful in the model cyanobacterium *Synechocystis* [19, 37, 38, 50] and the green algal model organisms *Chlorella vulgaris* [38] and *Chlamydomonas reinhardtii* [51, 52], but rarely applied for diagnostic purposes in other microalgae that have high relevance in applied research. As employed here, the integrated cuvette-based photosynthesis analysis system allows recording NADPH kinetics without disturbing the physiological state of the sample or changing the geometry of the setup, therefore screening of NADPH fluorescence-based traits can be performed at customarily selected time points of the experiment. Initial fluorescence was measured in the dark for 30 s to obtain the steady state level of the NADP pool. An initial rise in NADPH fluorescence at the onset of actinic illumination represents light-driven NADP reduction via linear electron flow, which is followed by a pronounced dip phase, before a second rise phase sets in (the complex phenomenon of the initial NADPH fluorescence kinetics is analyzed and described in [19, 37–39]). NADPH fluorescence exhibits a local maximum at around about 20 s (Nm), followed by a fluorescence decrease due to NADPH consumption by activation of the CBB cycle for CO_2 fixation and then attains a plateau phase during which NADPH production and consumption are in equilibrium (Nt). Under Ci-replete condition, NADPH fluorescence declines from the Nm to Nt phase within about 50 s, indicating the high uptake capacity of these NADPH-utilizing pathways. After turning off the actinic light, a sharp decline in NADPH fluorescence could be observed, as LEF ceases to drive electrons for reducing $NADP^+$, but the NADPH consumption pathways remain active due to the uptake of NADPH via the CBB cycle, resulting in an undershoot of the NADPH signal. The 'undershoot' signal plateaued within about 15–20 s, in agreement with the time course of cessation of CO_2 assimilation in the darkness after illumination (e.g. [53]). Finally, NADPH fluorescence recovers to the initial dark-adapted state due to the filling up of the NADPH pool e.g. via the reductive pentose phosphate pathway [37].

In *Synechocystis* grown at 3% CO_2, a marked change could be observed during the transition from Ci-replete to -depleted stage; the decline from Nm to Nt was less expressed, indicating the decreased NADPH uptake capacity by the CBB cycle (Fig 5A). This was partially recovered after adding 10 mM $NaHCO_3$, and the overall NADPH fluorescence intensity was also observed to decrease, probably because of the elevated rate of NADPH consumption over NADPH production upon repletion of the cells with Ci [19]. *Synechocystis* cells grown at ambient CO_2 (Fig 5B) showed an elevated NADPH fluorescence in the initial Ci-replete state (resuspended in BG11 medium), the first rapid dip in fluorescence was diminished, and the Nm-Nt fluorescence difference decreased, indicating that the cells entered the Ci-limited stage. Under prolonged Ci limitation, the first dip in NADPH fluorescence was absent. Addition of $NaHCO_3$ restored the Ci-replete 'phenotype', as the fast fluorescence dip reappeared and the Nm-Nt difference became more pronounced (and the overall NADPH fluorescence decreased), indicating a regained CBB cycle activity based on NADPH fluorescence signature (Fig 5B). It has to be noted that the initial rapid changes in NADPH fluorescence kinetics (in the first 50 s timescale after the onset of AL) cannot be assigned to the activity of the CBB cycle, because the activation of the CBB cycle is a slower reaction; Rubisco activation and CO_2 assimilation rates attain their maxima within a few minutes [54, 55]. Moreover, application of the CBB cycle inhibitor glycolaldehyde (GA) did not affect NADPH fluorescence kinetics significantly in the short (<min) timescale but inhibited the NADPH fluorescence decrease after the Nm phase, indicating that NADPH uptake by the CBB cycle was impaired (S9 Fig).

In the case of the M55 mutant (Fig 5C), AL caused only a minor transient increase in NADPH fluorescence, but the NADPH fluorescence level rapidly decreased below the initial

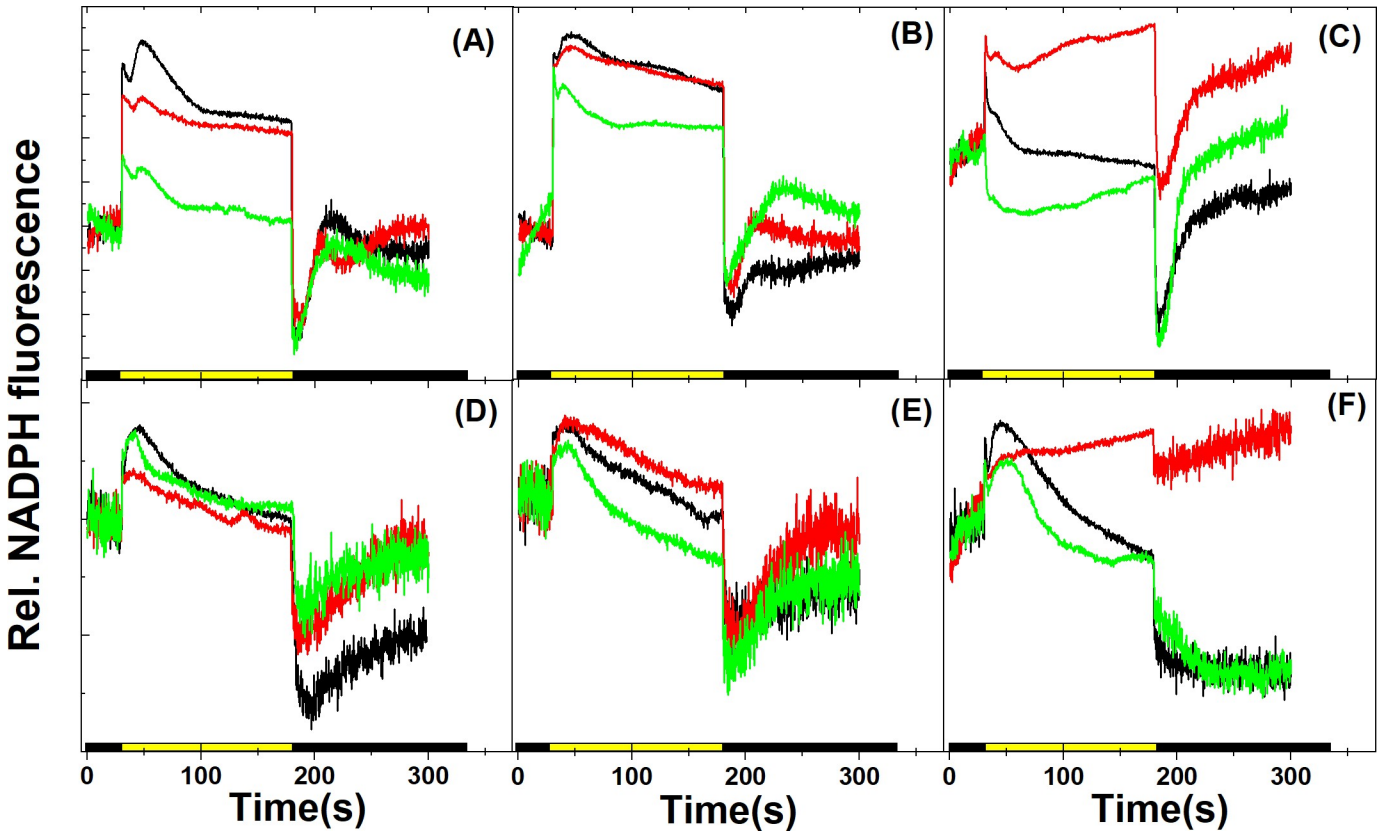

Fig 5. NADPH fluorescence kinetics traces in Ci-replete (black), -depleted (red) and recovery (green) states during the course of Ci limitation, for all species and conditions. Cells were dark-adapted for 3 min before each measurement. Data acquisition was started in the dark, followed by illumination with actinic red light at ~56 μmol photons m^{-2} s^{-1}, and was finished in darkness, as indicated by the black, yellow, and black bars on the X axis, respectively. The first 30 s of traces were measured in the dark, actinic light was turned on at 30 s and turned off at 180 s, and the light-to-dark changes were measured up to 300 s. (A) *Synechocystis* sp. PCC6803 WT grown at 3% CO_2, (B) *Synechocystis* sp. PCC6803 WT grown at ambient CO_2, (C) *Synechocystis M55* mutant, (D) *Chlorella sorokiniana*, (E) *Nannochloropsis limnetica*, (F) *Dunaliella salina*. Each trace represents the average of three replicates.

https://doi.org/10.1371/journal.pone.0236188.g005

dark-adapted level, and a rapid decrease after illumination also occurred. In Ci-limited stage, the light-induced NADPH fluorescence increase was present, however the dip during the illumination period was diminished, consequently Nt was at a much higher level than in the Ci-replete control. After replenishing M55 cells with $NaHCO_3$, the initial Ci-replete 'phenotype' was even more expressed, i.e. the complete lack of the light-induced transient increase was accompanied with a very pronounced decrease below the initial level during AL and the undershoot of the NADPH fluorescence signal after illumination. The absence of NADPH uptake by the CBB cycle during actinic illumination in Ci-depleted phase is in agreement with previous studies in the M55 mutant; it was observed that when the CBB cycle was chemically blocked, light-induced NADPH formation was not significantly influenced, but NADPH uptake during light in 1–2 min timescale was retarded [37]. However, the current study also reveals that in the Ci-limited phase in the M55 mutant the light-induced increase in NADPH fluorescence was more expressed than in the Ci-replete state. This is possibly due to the fact that in M55 the NADPH level in the dark was lower in Ci-depleted than in Ci-replete state (and so, the 'phenotype' of Ci-limited M55 cells resembled the 'phenotype' of WT cells in Ci-depleted state).

The NADPH fluorescence phenomenology exhibited similar patterns in eukaryotic microalgae as well; the characteristic initial rise, a transient dip, a secondary rise to a peak (Nm)

followed by a decrease upon CBB activation could be observed, in agreement with previous studies on NADPH fluorescence kinetics in *C. vulgaris* [38]; however, minor differences in different species could also be identified. Light-induced NADPH fluorescence changes were the most sensitive to Ci limitation in *D. salina* (Fig 5F). The fluorescence signal nearly flattened upon Ci depletion with significant loss in both light-induced NADPH fluorescence increase and Nm-Nt difference, and the post-illumination fluorescence decrease was diminished as well. These changes were nearly completely reversible upon Ci repletion. In the species *C. sorokiniana* and *N. limnetica* (Fig 5D and 5E, respectively) light-induced NADPH fluorescence kinetics and its changes during transition from Ci-replete to -depleted state (and recovery after $NaHCO_3$ addition) exhibited similar properties (i.e. the flattening of NADPH fluorescence from Nm to Nt under Ci depletion, which was partially reversible after addition of $NaHCO_3$). However, these changes were less characteristic as compared to *D. salina* and *Synechocystis*, even though the onset of Ci limitation based on PSII quantum yield and cessation of oxygen evolution (see above) was evident. This indicates that alternative NADPH oxidation mechanisms might be operational even when NADPH oxidation by the CBB cycle under Ci limitation is hampered (e.g. [56]), and these multiple mechanisms might contribute to NADPH uptake kinetics to different extents in the different species. Therefore, although the NADPH fluorescence phenomenology is a sensitive marker of rapid changes in the Ci status of cells, further studies are required to fully elucidate its applicability under various physiological conditions in green and eustigmatophycean algae.

Chlorophyll fluorescence induction-recovery kinetics under Ci limitation

Chlorophyll fluorescence kinetics were recorded in parallel with NADPH fluorescence kinetics, therefore this combined approach allowed a close monitoring of changes in photosynthetic electron transport under Ci limitation. After switching on the actinic light, an increase in chlorophyll fluorescence was observed, the kinetics of which was complex and the underlying phenomena are not fully resolved here. In general, it is related to progressive reduction and reoxidation of quinone electron acceptors (mainly Q_A and PQ), which reflects a quasi-steady state balance of rates corresponding to the actinic excitation rate generating Q_A^- (Q_A reduction rate) and the rate of forward electron transfer of electron into the PQ pool via the PSII Q_B site (Q_A^-oxidation rate) [57, 58]. Upon prolonged illumination (30 s– 150 s) the chlorophyll fluorescence declines, as PQ becomes oxidized due to the activation of photochemical quenching and the CBB cycle (this phase also corresponds to the initiation of NADPH uptake by the CBB cycle (see Fig 5). Upon switching off the actinic light at 180 s, chlorophyll fluorescence displays fluctuations with multiple peaks on different timescales, which are related to the redox changes in the PQ pool, mediated by the electron transport carriers from the cytosol to the chloroplast stroma [19, 59, 60]. The fast phase of post-illumination rise was observed within 1–10 s after actinic light was switched off in *Synechocystis* PCC 6803 WT: this post-illumination rise can be attributed to the operation of the cyclic electron flow [19]. In *Synechocystis* PCC 6803 WT (grown at 3% CO_2) the post-illumination rise was observed within 3–5 s in both in Ci-replete and -depleted state, and it was diminished in the Ci recovery phase (Fig 6A). *Synechocystis* cells grown at ambient CO_2 expressed faster post-illumination rise kinetics within 1–3 s (in agreement with [60]), the amplitude of which, however, did not change during the prolonged Ci limitation phase (Fig 6B). Post-illumination fluorescence rise was completely missing in the mutant M55, irrespectively of Ci content (Fig 6C), in agreement with previous studies (e.g. [61]). A slower post-illumination fluorescence rise signal in the timescale of 20–50 s was also observed earlier in *Synechocystis* and was denoted as F_R, which could be assigned to enhanced reductant flow to the PQ pool because of the accumulation of reduced carbon skeletons from

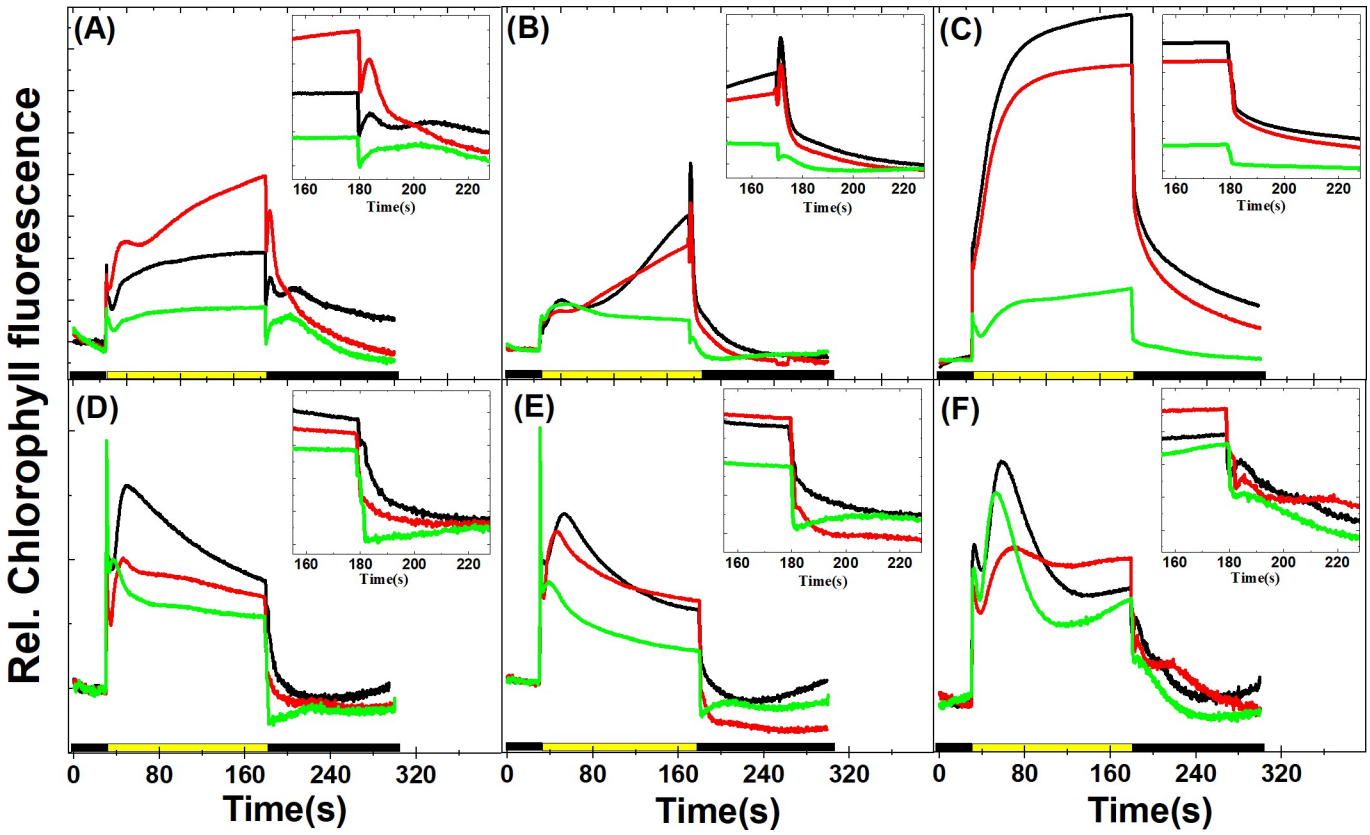

Fig 6. Chlorophyll fluorescence induction kinetics traces in Ci-replete (black), -depleted (red) and recovery (green) states during the course of Ci limitation. The first 30 s of traces were measured in the dark, actinic light (~56 μmol photons m^{-2} s^{-1}) was turned on at 30 s and turned off at 180 s, and subsequently post-illumination kinetics was measured up to 300 s. (A) *Synechocystis* sp. PCC6803 WT grown at 3% CO_2, (B) *Synechocystis* sp. PCC6803 WT grown at ambient CO_2, (C) *Synechocystis M55* mutant, (D) *Chlorella sorokiniana*, (E) *Nannochloropsis limnetica*, (F) *Dunaliella salina*. The insets in each panel show the post-illumination chlorophyll fluorescence rise during the light to dark transition period. Each trace represents the average of three replicates.

https://doi.org/10.1371/journal.pone.0236188.g006

the operation of the CBB cycle [59]. *Synechocystis* grown at 3% CO_2 displayed this slow rise in the initial Ci-replete stage, but it was particularly expressed after addition of $NaHCO_3$ after the Ci-depleted phase (inset of Fig 6A, in agreement with [59]). In *Synechocystis* grown at ambient CO_2 this slow rise was less expressed, as the post-illumination rise was dominated by the faster component, likely attributable to elevated CEF. After addition of $NaHCO_3$, the fast post-illumination component disappeared and, interestingly, the slow F_R peak could not be observed either. However, a smaller and faster post-illumination component remained (Fig 6B inset), indicating altered reductant flow under ambient CO_2 cultivation and possibly also due to a higher reduction state of the PQ pool (see below). Based on the above findings, Chl fluorescence characteristics at different stages of actinic illumination and after cessation of illumination could be a simple indicator of Ci status and possibly also the indicator of the PQ pool's redox state mediated by the carbohydrate biosynthesis pathways in cyanobacteria.

The Chl fluorescence induction kinetics was more complex in microalgae, and the results presented in the current study do not allow a detailed interpretation of the underlying mechanisms. Nevertheless, in general it can be concluded that the fast post-illumination rise signal, indicative of elevated CEF capacity under Ci limitation, could not be observed in *C. sorokiniana* and *N. limnetica* (Fig 6D and 6E, respectively), possibly because alternative mechanisms (pseudo-cyclic electron transport mechanisms, Mehler reaction, plastidial terminal oxidase) compete with CEF and therefore CEF-mediated PQ reduction is alleviated. *D. salina* (Fig 6F)

exhibited a small but apparent post-illumination rise, which was more pronounced in Ci-depleted phase and disappeared after $NaHCO_3$ treatment. The appearance of the slow component of the fluorescence rise (20–40 s) after addition of $NaHCO_3$ was apparent in *C. sorokiniana* and *N. limnetica* (inset of Fig 6D and 6E, respectively). The multi-phasic fluorescence oscillation pattern appeared to behave differently in *D. salina*; in this species a slow component could also be observed in Ci-limited phase, whereas in the initial and recovery phases fluorescence decreased monotonically without exhibiting any post-illumination peaks (Fig 6F inset). Therefore, the multiple components of fluorescence oscillations could be employed for obtaining information about the rapid regulation of electron transport (such as CEF), as well as the redox changes associated with carbohydrate metabolism in eukaryotic algae.

Analysis of forward electron transfer kinetics under Ci limitation

Flash-induced chlorophyll fluorescence decay curves give information about the re-oxidation kinetics of Q_A^- via forward electron transfer to Q_B and the PQ pool, or recombination with the donor side of PSII. The relaxation is dominated by a fast phase (~300–500 μs) that reflects electron transfer from Q_A^- to Q_B (Q_B^-). The middle phase (~5–15 ms) arises from reoxidation of Q_A^- by PQ that binds to the Q_B site after flash, whereas the slow phase (~10–20 s) arises from the $S_2Q_AQ_B^-$ charge recombination [15]. Flash-induced fluorescence decay profiles showed a slightly higher fluorescence level in Ci-depleted stage in *Synechocystis* PCC6803 WT (grown with and without CO_2) on the 5–500 ms timescale (Fig 7A and 7B). In the M55 mutant (Fig

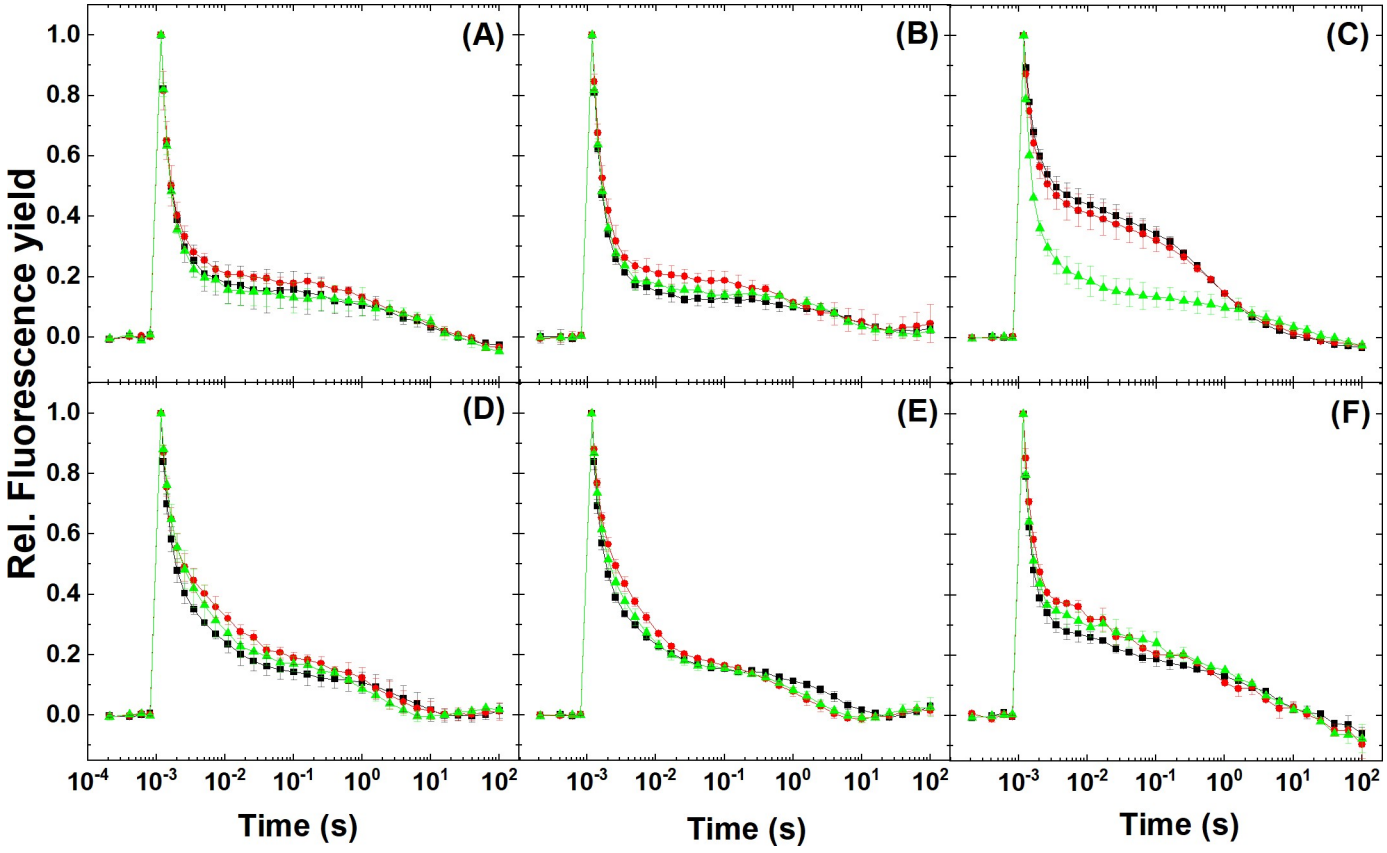

Fig 7. Flash-induced chlorophyll fluorescence decay curve traces at Ci-replete (black), -depleted (red) and recovery (green) stages undergoing Ci limitation. (A) *Synechocystis* sp. PCC6803 WT grown at 3% CO_2, (B) *Synechocystis* sp. PCC6803 WT grown at ambient CO_2, (C) *Synechocystis M55* mutant, (D) *Chlorella sorokiniana*, (E) *Nannochloropsis limnetica*, (F) *Dunaliella salina*. Traces represent the average of 3 replicates.

https://doi.org/10.1371/journal.pone.0236188.g007

7C) the fluorescence decay was slow and the fluorescence level remained high in the 2 ms-1 s timescale in the initial Ci-replete state and the progression to Ci-limited stage did not change this pattern, indicating that the electron transport capacity was limited, in agreement with the low effective quantum yield of PSII (Fig 3) and O_2 evolution capacity (Fig 4) under this condition. However, a fast decay is regained after addition of $NaHCO_3$, in agreement with the restoration of linear electron flow and O_2 evolving capacity (c.f. Figs 3 and 4, respectively). *Chlorella sorokiniana* and *Dunaliella salina* in the 2 ms-1 s region (Fig 7D and 7F, respectively) and *Nannochloropsis limnetica* in the 2–20 ms region (Fig 7E) showed similar patterns after Ci limitation, which indicated a limited capacity of reoxidation of Q_A^- by the PQ molecules bound to the Q_B site after the flash [15] under Ci-limited condition. These changes were largely reversible after addition of $NaHCO_3$, in agreement with previous studies that showed the restoration of electron flow between Q_A^- to Q_B after addition of 10 mM $NaHCO_3$ to bicarbonate-depleted cells [62, 63]. Taken together, flash fluorescence decay signals indicated slightly decreased capacity of Q_A^- reoxidation by the PQ molecules under Ci-limited condition in all species and conditions, although these changes appeared to be minor under the conditions investigated here.

The polyphasic rise of chlorophyll fluorescence, or commonly referred to as OJIP curves, is a frequently used method to investigate fast dynamic changes in various components of the photosynthetic electron transport chain and PSII efficiency from dark to light transition (e.g. [64, 65]). Transient chlorophyll *a* fluorescence rise is induced during a dark-to-strong light transition, where O is equivalent to F_0, P is for peak, equivalent to F_m (when measured at saturating light) and J and I (or F_J and F_I) are inflection points typically at 2 and 30 ms, respectively, between O and P. The O-J fluorescence rise is the photochemical phase reflecting the closure of open reaction centers, where the PSII electron acceptors Q_A and Q_B become fully reduced, and the reduction of Q_A and the reoxidation of Q_A^- by PQ molecules are in equilibrium at the J step (2–3 ms). The J-I phase is a dip due to the partial reduction of intersystem electron carriers Q_B, PQ, Cyt b_6/f (mainly the PQ pool) and the electron transfer towards the PSI, and the I-P phase is determined by electron carriers PQH_2, PC^+, $P700^+$ and PSI electron acceptors (such as FNR activity) [66, 67]). In ambient CO_2-grown *Synechocystis* (Fig 8B), the J phase was relatively high as compared to *Synechocystis* grown at 3% CO_2 (Fig 8A), indicating a slower Q_A^- reoxidation by PQ molecules. The onset of Ci limitation from the initial Ci-replete state caused an elevated J step, which was reversible after $NaHCO_3$ addition. The increase in J step under Ci limitation was not significant in 3% CO_2 grown *Synechocystis*. The M55 mutant (Fig 8C) already exhibited a high J step in the Ci-replete state, which did not change in Ci-limited state; however, it significantly dropped after $NaHCO_3$ addition as a result of the restoration of active electron transport (c.f. Figs 3, 4 and 7 and also S3 Fig). The increase in J step under Ci limitation was also observed in eukaryotic microalgae (Fig 8D–8F), which partially or fully recovered upon $NaHCO_3$ addition, although the changes in the O-J-I-P phases appeared to be significant only in the *Synechocystis* M55 mutant after $NaHCO_3$ addition (the original OJIP transients and transients normalized to the F_0 level are shown in Supplementary Material S10 and S11 Figs). These results indicate that the OJIP transients are informative to reveal species- and condition-specific patterns, although the induced CO_2 limitation exerted only minor effects on Q_A^- reoxidation, except in the M55 mutant of *Synechocystis* (in agreement with the flash-induced fluorescence decay patterns, Fig 7).

Conclusions

The cuvette system presented in the current study enabled simultaneous real-time monitoring of several parameters that are indicative of the physiological status of the photosynthetic

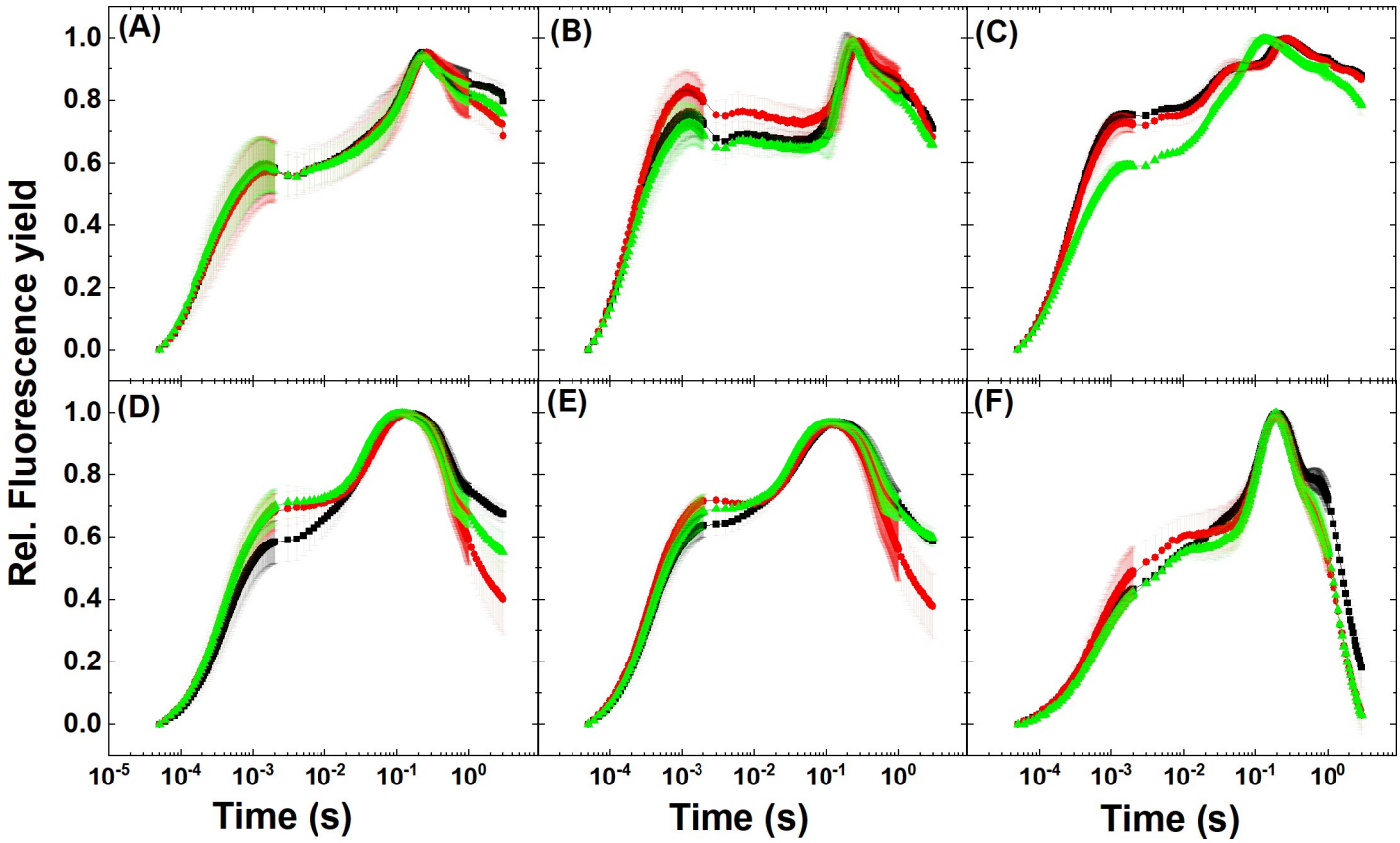

Fig 8. OJIP transients at Ci-replete (black), -depleted (red) and recovery (green) stage undergoing Ci limitation. Cells were dark-adapted for 3 min before each measurement. (A) *Synechocystis* sp. PCC6803 WT grown at 3% CO_2, (B) *Synechocystis* sp. PCC6803 WT grown at ambient CO_2, (C) *Synechocystis M55* mutant, (D) *Chlorella sorokiniana*, (E) *Nannochloropsis limnetica*, (F) *Dunaliella salina*. Traces represent the average of 3 replicates.

https://doi.org/10.1371/journal.pone.0236188.g008

apparatus of cyanobacteria and microalgae. Photosynthetic characterization of the frequently applied model cyanobacterium *Synechocystis* sp. PCC6803 under transient CO_2 limitation showed that the integrated cuvette system is applicable to decipher distinct traits of this model species grown under different CO_2 regimes (also in agreement with some of the findings by [13, 19]). Moreover, the ndhB-deficient M55 mutant, which lacks all NDH-1 complexes (and is therefore unable to perform CEF and CCM) exhibited very clear phenotypic differences in Ci-replete vs. -depleted state. Although the M55 mutant has been thoroughly characterized in the past (e.g. [37, 68–70] reviewed in [71, 72]), applying this mutant in our studies was an important validation of the suitability of real-time monitoring of several photosynthetic parameters (changes in O_2 and Y(II) dynamics), along with alterations of NADPH synthesis/uptake kinetics, the redox state of the PQ pool and forward electron transfer kinetics in different Ci conditions. Therefore, this system is potentially applicable to the detection of subtle real-time changes in other *Synechocystis* mutants. Our results with *Synechocystis* allowed to extend physiological monitoring to other species of eukaryotic algae, by measuring not only the absolute values of PSII quantum yield and/or oxygen evolution rates at arbitrarily selected time points, but also the dynamic changes of photosynthetic parameters in algal suspensions subjected to various inorganic carbon regimes (e.g. onset, early and prolonged Ci limitation and kinetics of recovery from these conditions upon Ci repletion). In addition to the comprehensive monitoring of photosynthetic parameters and recording the extracellular pH in the

medium (using a pH microsensor), the integrated cuvette system presented here can be extended with highly sensitive detection of CO_2 (using membrane inlet mass spectrometry) and dynamic modelling of carbon chemistry. In this way the exchange of inorganic carbon species and the details of the inorganic carbon cycling (e.g. [73]) could also be revealed in future studies. These integrative approaches would therefore facilitate screening for stress- or condition-specific traits in industrially important microalgae and cyanobacteria.

Supporting information

S1 Table. Original absorbance readings of acetone:DMSO pigment extracts and the calculated Chl *a* and Chl *b* content, total Chl (*a*+*b*) content and the Chl *a*/*b* ratio. Eq 1 was used for calculating Chl *a* and Eq 2 was used for calculating Chl *b*.

Chl *a* ($\mu g\ mL^{-1}$) = $11.75^{*}A_{663}-2.35^{*}A_{645}$ (1)

Chl *b* ($\mu g\ mL^{-1}$) = $18.61^{*}A_{645}-3.96^{*}A_{663}$ (2)

[#]In *N*. *limnetica* the calculated Chl *b* content and Chl a/b ratio cannot be accurately interpreted due to the lack of Chl *b*.

(DOCX)

S1 Fig. Representative graph of physiological response of *Synechocystis* sp. PCC 6803 WT (3% CO_2 grown) during the course of Ci limitation. Simultaneous measurements of (A) Oxygen evolution and (B) Effective quantum yield of PSII (Y(II)) and (C) pH were performed. Y(II) and pH was measured every 5 min. The cells were kept in the dark for 30 min (grey shade region) then illuminated with actinic white light at 56 μmol photons $m^{-2}\ s^{-1}$. The dots in panel A represent the defined measuring time points of chlorophyll and NADPH fluorescence kinetics at: T0 (control) after 3 min in the dark; T1—initial Ci-replete phase (30 min) in the light; T2—early phase of Ci depletion (135 min); T3—prolonged Ci-depleted phase (240 min); T4—Ci recovery phase (265 min) in the light (arrow indicates the addition of 10 mM $NaHCO_3$).

(DOCX)

S2 Fig. Representative graph of physiological response of *Synechocystis* sp. PCC 6803 WT (Ambient CO_2 grown) during the course of Ci limitation. (A) Simultaneous measurements of A) Oxygen evolution and (B) Effective quantum yield of PSII (Y(II)) and (C) pH were performed. Y(II) and pH was measured every 5 min. The cells were kept in the dark for 25 min (grey shade region) then illuminated with actinic white light at 56 μmol photons $m^{-2}\ s^{-1}$. The dots in panel A represent the defined measuring time points of chlorophyll and NADPH fluorescence kinetics at: T0 (control) after 3 min in the dark; T1—initial Ci-replete phase (50 min in the light); T2—early phase of Ci depletion (125 min in the light); T3—prolonged Ci-depleted phase (230 min); T4—Ci recovery phase (270 min) in the light (arrow indicates the addition of 10 mM $NaHCO_3$).

(DOCX)

S3 Fig. Representative graph of physiological response of *Synechocystis* M55 mutant during the course of Ci limitation. Simultaneous measurements of (A) Oxygen evolution and (B) Effective quantum yield of PSII (Y(II)) and (C) pH were performed. Y(II) and pH was measured every 5 min. The cells were kept in the dark for 20 min (grey shade region) then illuminated with actinic white light at 56 μmol photons $m^{-2}\ s^{-1}$. The dots in panel A represent the defined measuring time points of chlorophyll and NADPH fluorescence kinetics at: T0 (control) after 3 min in the dark; T1—initial Ci-replete phase (55 min) in the light; T2—prolonged Ci-depleted phase (125 min in the light); T3—Ci recovery phase (175 min) in the light (arrow

indicates the addition of 10 mM $NaHCO_3$).
(DOCX)

S4 Fig. Representative graph of physiological response of *Chlorella sorokiniana* the course of Ci limitation. Simultaneous measurements of (A) Oxygen evolution and (B) Effective quantum yield of PSII (Y(II)) and (C) pH were performed. Y(II) and pH was measured every 5 min. The cells were kept in the dark for 20 min (grey shade region) then illuminated with actinic white light at 56 μmol photons m^{-2} s^{-1}. The dots in panel A represent the defined measuring time points of chlorophyll and NADPH fluorescence kinetics at: T0 (control) after 3 min in the dark; T1—initial Ci-replete phase (80 min) in the light; T2—early phase of Ci depletion (170 min); T3—prolonged Ci-depleted phase (300 min); T4—Ci recovery phase (335 min) in the light (arrow indicates the addition of 10 mM $NaHCO_3$).
(DOCX)

S5 Fig. Representative graph of physiological response of *Nannochloropsis limnetica* during the course of Ci limitation. Simultaneous measurements of (A) Oxygen evolution and (B) Effective quantum yield of PSII (Y(II)) and (C) pH were performed. Y(II) and pH was measured every 5 min. The cells were kept in the dark for 20 min (grey shade region) then illuminated with actinic white light at 56 μmol photons m^{-2} s^{-1}. The dots in panel A represent the defined measuring time points of chlorophyll and NADPH fluorescence kinetics at: T0 (control) after 3 min in the dark; T1—initial Ci-replete phase (125 min) in the light; T2—early phase of Ci depletion (240 min); T3—prolonged Ci-depleted phase (370 min); T4—Ci recovery phase (420 min) in the light (arrow indicates the addition of 10 mM $NaHCO_3$).
(DOCX)

S6 Fig. Representative graph of physiological response of *Dunaliella salina* during the course of Ci limitation. Simultaneous measurements of (A) Oxygen evolution and (B) Effective quantum yield of PSII (Y(II)) and (C) pH were performed. Y(II) and pH was measured every 5 min. The cells were kept in the dark for 40 min (grey shade region) then illuminated with actinic white light at 56 μmol photons m^{-2} s^{-1}. The dots in panel A represent the defined measuring time points of chlorophyll and NADPH fluorescence kinetics at: T0 (control) after 3 min in the dark; T1—initial Ci-replete phase (85 min) in the light; T2—early phase of Ci depletion (180 min); T3—prolonged Ci-depleted phase (280 min); T4—Ci recovery phase (335 min) in the light (arrow indicates the addition of 10 mM $NaHCO_3$).
(DOCX)

S7 Fig. Oxygen evolution rate and electron transport rate (ETR) during the course of Ci limitation. Representative traces of the first derivatives of oxygen evolution (O_2, black) and ETR (red). The blue arrow represents the time of $NaHCO_3$ addition. (A) *Synechocystis* sp. PCC 6803 WT grown at 3% CO_2, (B) *Synechocystis* sp. PCC 6803 WT grown at ambient CO_2, (C) *Synechocystis* M55 mutant, (D) *Chlorella sorokiniana*, (E) *Nannochloropsis limnetica*, (F) *Dunaliella salina*
(DOCX)

S8 Fig. Representative chlorophyll fluorescence traces during the course of Ci limitation. The blue arrow represents the time of $NaHCO_3$ addition. (A) *Synechocystis* sp. PCC 6803 WT grown at 3% CO_2, (B) *Synechocystis* sp. PCC 6803 WT grown at ambient CO_2, (C) *Synechocystis* M55 mutant, (D) *Chlorella sorokiniana*, (E) *Nannochloropsis limnetica*, (F) *Dunaliella salina*
(DOCX)

S9 Fig. Representative NADPH fluorescence traces of WT *Synechocystis* sp. PCC 6803 WT in the absence (black line) or presence (red line) of 10 mM GA. Cells were grown in the

presence of 3% CO_2 (as described in Materials and Methods) and dark adapted for 5 min before the measurements.
(DOCX)

S10 Fig. Representative original OJIP traces (not normalized) at Ci-replete (black), -depleted (red) and recovery (green) stage undergoing Ci limitation. Cells were dark adapted 3min before every measurement. (A) *Synechocystis* sp. PCC 6803 WT grown at 3% CO_2, (B) *Synechocystis* sp. PCC 6803 WT grown at ambient CO_2, (C) *Synechocystis* M55 mutant, (D) *Chlorella sorokiniana*, (E) *Nannochloropsis limnetica*, (F) *Dunaliella salina*.
(DOCX)

S11 Fig. Representative OJIP traces that were normalized to F_0 level (at 50 μs timepoint) at Ci-replete (black), -depleted (red) and recovery (green) stage undergoing Ci limitation. Cells were dark adapted 3min before every measurement. (A) *Synechocystis* sp. PCC 6803 WT grown at 3% CO_2, (B) *Synechocystis* sp. PCC 6803 WT grown at ambient CO_2, (C) *Synechocystis* M55 mutant, (D) *Chlorella sorokiniana*, (E) *Nannochloropsis limnetica*, (F) *Dunaliella salina*.
(DOCX)

Author Contributions

Conceptualization: Imre Vass, Milán Szabó.

Formal analysis: Priyanka Pradeep Patil.

Funding acquisition: Milán Szabó.

Investigation: Priyanka Pradeep Patil, Sandeesha Kodru.

Methodology: Priyanka Pradeep Patil, Milán Szabó.

Project administration: Milán Szabó.

Resources: Imre Vass.

Supervision: Milán Szabó.

Visualization: Priyanka Pradeep Patil.

Writing – original draft: Priyanka Pradeep Patil, Imre Vass, Sandeesha Kodru, Milán Szabó.

Writing – review & editing: Imre Vass, Milán Szabó.

References

1. Kramer DM, Evans JR. The importance of energy balance in improving photosynthetic productivity. Plant Physiol. 2011; 155: 70–78. https://doi.org/10.1104/pp.110.166652 PMID: 21078862
2. Cardol P, Forti G, Finazzi G. Regulation of electron transport in microalgae. Biochim Biophys Acta. 2011; 1807: 912–918. https://doi.org/10.1016/j.bbabio.2010.12.004 PMID: 21167125
3. Peltier G, Aro E, Shikanai T. NDH-1 and NDH-2 Plastoquinone Reductases in oxygenic photosynthesis. Annu Rev Plant Biol. 2016; 67: 55–80. https://doi.org/10.1146/annurev-arplant-043014-114752 PMID: 26735062
4. Baker NR, Harbinson J, Kramer DM. Determining the limitations and regulation of photosynthetic energy transduction in leaves. Plant Cell Environ. 2007; 30: 1107–1125. https://doi.org/10.1111/j.1365-3040.2007.01680.x PMID: 17661750
5. Huertas IE, Espie GS, Colman B, Lubian LM. Light-dependent bicarbonate uptake and CO2 efflux in the marine microalga *Nannochloropsis gaditana*. Planta. 2000; 211: 43–49. https://doi.org/10.1007/s004250000254 PMID: 10923702

6. Burnap RL, Hagemann M, Kaplan A. Regulation of CO2 concentrating mechanism in cyanobacteria. Life. 2015; 5: 348–371. https://doi.org/10.3390/life5010348 PMID: 25636131

7. Price GD, Badger MR, Woodger FJ, Long BM. Advances in understanding the cyanobacterial CO2-concentrating- mechanism (CCM): Functional components, Ci transporters, diversity, genetic regulation and prospects for engineering into plants. J Exp Bot. 2008; 59: 1441–1461. https://doi.org/10.1093/jxb/erm112 PMID: 17578868

8. Raven JA, Beardall J, Giordano M. Energy costs of carbon dioxide concentrating mechanisms in aquatic organisms. Photosynth Res. 2014; 121: 111–124. https://doi.org/10.1007/s11120-013-9962-7 PMID: 24390639

9. Kalaji HM, Schansker G, Ladle RJ, Goltsev V, Bosa K, Allakhverdiev SI, et al. Frequently asked questions about in vivo chlorophyll fluorescence: Practical issues. Photosynth Res. 2014; 122: 121–158. https://doi.org/10.1007/s11120-014-0024-6 PMID: 25119687

10. Baker NR. Chlorophyll Fluorescence: A probe of photosynthesis in vivo. Annu Rev Plant Biol. 2008; 59: 89–113. https://doi.org/10.1146/annurev.arplant.59.032607.092759 PMID: 18444897

11. Spalding MH, Critchley C, Govindjee, Orgren WL. Influence of carbon dioxide concentration during growth on fluorescence induction characteristics of the green alga *Chlamydomonas reinhardii*. Photosynth Res. 1984; 5: 169–176. https://doi.org/10.1007/BF00028529 PMID: 24458604

12. Schreiber U, Bilger W, Neubauer C. Chlorophyll fluorescence as a nonintrusive indicator for rapid assessment of in vivo photosynthesis. In: Schulze E-D, Caldwell MM, editors. Ecophysiology of Photosynthesis. Berlin, Heidelberg: Springer Berlin Heidelberg; 1995. pp. 49–70. https://doi.org/10.1007/978-3-642-79354-7_3

13. Shimakawa G, Akimoto S, Ueno Y, Wada A, Shaku K, Takahashi Y, et al. Diversity in photosynthetic electron transport under [CO_2] —limitation: the cyanobacterium *Synechococcus* sp. PCC 7002 and green alga *Chlamydomonas reinhardtii* drive an O_2 -dependent alternative electron flow and non-photochemical quenching of chlorophyll fluorescence during CO_2-limited photosynthesis. Photosynth Res. 2016; 130: 293–305. https://doi.org/10.1007/s11120-016-0253-y PMID: 27026083

14. Shimakawa G, Shaku K, Miyake C. Reduction-induced suppression of electron flow (RISE) is relieved by non-ATP-consuming electron flow in *Synechococcus elongatus* PCC 7942. Front Microbiol. 2018; 9: 1–11. https://doi.org/10.3389/fmicb.2018.00001 PMID: 29403456

15. Deák Z, Sass L, Kiss É, Vass I. Characterization of wave phenomena in the relaxation of flash-induced chlorophyll fluorescence yield in cyanobacteria. Biochim Biophys Acta—Bioenerg. 2014; 1837: 1522–1532. https://doi.org/10.1016/j.bbabio.2014.01.003 PMID: 24434028

16. Krishna PS, Morello G, Mamedov F. Characterization of the transient fluorescence wave phenomenon that occurs during H2 production in *Chlamydomonas reinhardtii*. J Exp Bot. 2019; 70: 6321–6336. https://doi.org/10.1093/jxb/erz380 PMID: 31504725

17. Lucker B, Kramer DM. Regulation of cyclic electron flow in *Chlamydomonas reinhardtii* under fluctuating carbon availability. Photosynth Res. 2013; 117: 449–459. https://doi.org/10.1007/s11120-013-9932-0 PMID: 24113925

18. Tamburic B, Evenhuis CR, Suggett DJ, Larkum AWD, Raven JA, Ralph PJ. Gas transfer controls carbon limitation during biomass production by marine microalgae. ChemSusChem. 2015; 8: 2727–2736. https://doi.org/10.1002/cssc.201500332 PMID: 26212226

19. Holland SC, Kappell AD, Burnap RL. Redox changes accompanying inorganic carbon limitation in *Synechocystis* sp. PCC 6803. Biochim Biophys Acta—Bioenerg. 2015; 1847: 355–363. https://doi.org/10.1016/j.bbabio.2014.12.001 PMID: 25490207

20. Ananyev G, Gates C, Dismukes GC. The oxygen quantum yield in diverse algae and cyanobacteria is controlled by partitioning of flux between linear and cyclic electron flow within photosystem II. Biochim Biophys Acta- Bioenerg. 2016; 1857: 1380–1391. https://doi.org/10.1016/j.bbabio.2016.04.056 PMID: 27117512

21. Ananyev G, Gates C, Dismukes GC. The multiplicity of roles for (bi)carbonate in photosystem II operation in the hypercarbonate-requiring cyanobacterium *Arthrospira maxima*. Photosynthetica. 2018; 56: 217–228. https://doi.org/10.1007/s11099-018-0781-0

22. Ogawa T. A gene homologous to the subunit-2 gene of NADH dehydrogenase is essential to inorganic carbon transport of Synechocystis PCC6803. Proc Natl Acad Sci U S A. 1991; 88: 4275–4279. https://doi.org/10.1073/pnas.88.10.4275 PMID: 1903537

23. Cournac L, Guedeney G, Peltier G, Vignais PM. Sustained photoevolution of molecular hydrogen in a mutant of *Synechocystis* sp. strain PCC 6803 deficient in the type I NADPH-dehydrogenase complex. J Bacteriol. 2004; 186: 1737–1746. https://doi.org/10.1128/jb.186.6.1737-1746.2003 PMID: 14996805

24. Cooley JW, Vermaas WF. Succinate dehydrogenase and other respiratory pathways in thylakoid membranes of *Synechocystis* sp. strain PCC 6803: capacity comparisons and physiological function. J Bacteriol. 2001; 183: 4251–4258. https://doi.org/10.1128/JB.183.14.4251-4258.2001 PMID: 11418566

25. De-Bashan LE, Trejo A, Huss VAR, Hernandez JP, Bashan Y. *Chlorella sorokiniana* UTEX 2805, a heat and intense, sunlight-tolerant microalga with potential for removing ammonium from wastewater. Bioresour Technol. 2008; 99: 4980–4989. https://doi.org/10.1016/j.biortech.2007.09.065 PMID: 18024023

26. Sun Z, Chen YF, Du J. Elevated CO2 improves lipid accumulation by increasing carbon metabolism in *Chlorella sorokiniana*. Plant Biotechnol J. 2016; 14: 557–566. https://doi.org/10.1111/pbi.12398 PMID: 25973988

27. Borowitzka MA. Dunaliella: Biology, production, and markets. In: Richmond A, Hu Q, editors. Handbook of Microalgal Culture. John Wiley & Sons, Ltd; 2013. pp. 359–368. https://doi.org/10.1002/9781118567166.ch18

28. Melis A, Neidhardt J, Benemann JR. Dunaliella salina (Chlorophyta) with small chlorophyll antenna sizes exhibit higher photosynthetic productivities and photon use efficiencies than normally pigmented cells. J Appl Phycol. 1998; 10: 515–525. https://doi.org/10.1023/A:1008076231267

29. Krienitz L, Hepperle D, Stich HB, Weiler W. *Nannochloropsis limnetica* (Eustigmatophyceae), a new species of picoplankton from freshwater. Phycologia. 2000; 39: 219–227. https://doi.org/10.2216/i0031-8884-39-3-219.1

30. Tamburic B, Guruprasad S, Radford DT, Szabó M, Lilley RM, Larkum AWD, et al. The effect of diel temperature and light cycles on the growth of *Nannochloropsis oculata* in a photobioreactor matrix. PLoS One. 2014; 9: e86047. https://doi.org/10.1371/journal.pone.0086047 PMID: 24465862

31. Tamburic B, Evenhuis CR, Crosswell JR, Ralph PJ. An empirical process model to predict microalgal carbon fixation rates in photobioreactors. Algal Res. 2018; 31: 334–346. https://doi.org/10.1016/j.algal.2018.02.014

32. Zavřel T, Szabó M, Tamburic B, Evenhuis C, Kuzhiumparambil U, Literáková P, et al. Effect of carbon limitation on photosynthetic electron transport in *Nannochloropsis oculata*. J Photochem Photobiol B Biol. 2018; 181: 31–43. https://doi.org/10.1016/j.jphotobiol.2018.02.020 PMID: 29486460

33. Lucker BF, Hall CC, Zegarac R, Kramer DM. The environmental photobioreactor (ePBR): An algal culturing platform for simulating dynamic natural environments. Algal Res. 2014; 6: 242–249. https://doi.org/10.1016/j.algal.2013.12.007

34. Dere S, Gunes T, Sivaci R. Spectrophotometric determination of chlorophyll—A, B and total carotenoid contents of some algae species using different solvents. Tr J Botany. 1998; 22: 13–18.

35. Shoaf WT, Lium BW. Improved extraction of chlorophyll a and b from algae using dimethyl sulfoxide. Limnol Oceanogr. 1976; 926–928. https://doi.org/10.4319/lo.1976.21.6.0926

36. Genty B, Briantais JM, Baker NR. The relationship between the quantum yield of photosynthetic electron transport and quenching of chlorophyll fluorescence. Biochim Biophys Acta. 1989; 990: 87–92. https://doi.org/10.1016/S0304-4165(89)80016-9

37. Mi H, Klughammer C, Schreiber U. Light-induced dynamic changes of NADPH fluorescence in *Synechocystis* PCC 6803 and its ndhB -defective mutant M55. Plant Cell Physiol. 2000; 41(10): 1129–1135. https://doi.org/10.1093/pcp/pcd038 PMID: 11148271

38. Schreiber U, Klughammer C. New NADPH / 9-AA module for the DUAL-PAM-100: Description, operation and examples of application. PAM Application Notes. 2009; 2: 1–13.

39. Kauny J, Sétif P. NADPH fluorescence in the cyanobacterium *Synechocystis* sp. PCC 6803: A versatile probe for in vivo measurements of rates, yields and pools. Biochim Biophys Acta—Bioenerg. 2014; 1837: 792–801. https://doi.org/10.1016/j.bbabio.2014.01.009 PMID: 24463053

40. Shimakawa G, Matsuda Y, Nakajima K, Tamoi M. Diverse strategies of O2 usage for preventing photooxidative damage under CO2 limitation during algal photosynthesis. Sci Rep. 2017; 7: 1–9. https://doi.org/10.1038/s41598-016-0028-x PMID: 28127051

41. Kirilovsky D. Modulating energy arriving at photochemical reaction centers: Orange carotenoid protein-related photoprotection and state transitions. Photosynth Res. 2015; 126: 3–17. https://doi.org/10.1007/s11120-014-0031-7 PMID: 25139327

42. Ananyev G, Nguyen T, Putnam-Evans C, Dismukes GC. Mutagenesis of CP43-arginine-357 to serine reveals new evidence for (bi) carbonate functioning in the water oxidizing complex of Photosystem II. Photochem Photobiol Sci. 2005; 4: 991–998. https://doi.org/10.1039/b507519j PMID: 16307112

43. Shevela D, Eaton-Rye JJ, Shen JR, Govindjee. Photosystem II and the unique role of bicarbonate: A historical perspective. Biochim Biophys Acta—Bioenerg. 2012; 1817: 1134–1151. https://doi.org/10.1016/j.bbabio.2012.04.003 PMID: 22521596

44. Klimov VV, Baranov SV. Bicarbonate requirement for the water-oxidizing complex of photosystem II. Biochim Biophys Acta—Bioenerg. 2001; 1503: 187–196. https://doi.org/10.1016/S0005-2728(00)00222-X

45. Wydrzynski T, Govindjee. A new site of bicarbonate effect in Photosystem II of photosynthesis: evidence from chlorophyll fluorescence transients in spinach chloroplasts. BBA Report. Biochim Biophys Acta. 1975; 387: 403–408. https://doi.org/10.1016/0005-2728(75)90121-8 PMID: 1125295

46. Van Rensen JJS. Role of bicarbonate at the acceptor side of Photosystem II. Photosynth Res. 2002; 73: 185–192. https://doi.org/10.1023/A:1020451114262 PMID: 16245121

47. Vermaas WFJ, Govindjee. Bicarbonate or carbon dioxide as a requirement for efficient electron transport on the acceptor side of Photosystem II. In: Govindjee, editor. Photosynthesis: Development, Carbon Metabolism, and Plant Productivity, Vol. II. Academic Press Inc. 1982. pp. 541–558.

48. Hayashi R, Shimakawa G, Shaku K, Shimizu S, Yamamoto H, Amako K, et al. O_2 -dependent large electron flow functioned as an electron sink, replacing the steady-state electron flux in photosynthesis in the cyanobacterium *Synechocystis* sp. PCC 6803, but not in the cyanobacterium *Synechococcus* sp. PCC 7942. Biosci Biotechnol Biochem. 2014; 78: 384–393. https://doi.org/10.1080/09168451.2014.882745 PMID: 25036824

49. Allahverdiyeva Y, Ermakova M, Eisenhut M, Zhang P, Richaud P, Hagemann M, et al. Interplay between flavodiiron proteins and photorespiration in *Synechocystis* sp. PCC 6803. J Biol Chem. 2011; 286: 24007–24014. https://doi.org/10.1074/jbc.M111.223289 PMID: 21602273

50. Holland S, Artier J, Miller N, Cano M, Yu J, Ghirardi M, et al. Impacts of genetically engineered alterations in carbon sink pathways on photosynthetic performance. Algal Res. 2016; 20. 87–99. https://doi.org/10.1016/j.algal.2016.09.021

51. Roach T, Sedoud A, Krieger-Liszkay A. Acetate in mixotrophic growth medium affects photosystem II in *Chlamydomonas reinhardtii* and protects against photoinhibition. Biochim Biophys Acta—Bioenerg. 2013; 1827: 1183–1190. https://doi.org/10.1016/j.bbabio.2013.06.004 PMID: 23791666

52. White S. Anandraj A, Trois C. NADPH Fluorescence as an indicator of hydrogen production in the green algae *Chlamydomonas reinhardtii*. Int J Hydrogen Energy. 2013; 39: 1640–1647. https://doi.org/10.1016/just.ijhydene.2013.11.016

53. Ruuska S, Andrews TJ, Badger MR, Hudson GS, Laisk A, Price GD, et al. The interplay between limiting processes in C3 photosynthesis studied by rapid-response gas exchange using transgenic tobacco impaired in photosynthesis. Aust J Plant Physiol. 1998; 25: 859–870. https://doi.org/10.1071/PP98079

54. Kaiser E, Morales A, Harbinson J, Heuvelink E, Prinzenberg AE, Marcelis LFM. Metabolic and diffusional limitations of photosynthesis in fluctuating irradiance in Arabidopsis thaliana. Sci Rep. 2016; 6: 31252. https://doi.org/10.1038/srep31252 PMID: 27502328

55. Yamori W, Masumoto C, Fukayama H, Makino A. Rubisco activase is a key regulator of non-steady-state photosynthesis at any leaf temperature and, to a lesser extent, of steady-state photosynthesis at high temperature. Plant J. 2012; 71: 871–880. https://doi.org/10.1111/j.1365-313X.2012.05041.x PMID: 22563799

56. Clowez S, Godaux D, Cardol P, Wollman FA, Rappaport F. The involvement of hydrogen-producing and ATP-dependent NADPH-consuming pathways in setting the redox poise in the chloroplast of *Chlamydomonas reinhardtii* in anoxia. J Biol Chem. 2015; 290: 8666–8676. https://doi.org/10.1074/jbc.M114.632588 PMID: 25691575

57. Campbell D, Hurry V, Clarke AK, Gustafsson P, Öquist G. Chlorophyll fluorescence analysis of cyanobacterial photosynthesis and acclimation. Microbiol Mol Biol Rev. 1998; 62: 667–683. https://doi.org/10.1128/mmbr.62.3.667–683.1998 PMID: 9729605

58. Papageorgiou GC, Tsimilli-Michael M, Stamatakis K. The fast and slow kinetics of chlorophyll a fluorescence induction in plants, algae and cyanobacteria: A viewpoint. Photosynth Res. 2007; 94: 275–290. https://doi.org/10.1007/s11120-007-9193-x PMID: 17665151

59. Artier J, Holland SC, Miller NT, Zhang M, Burnap RL. Synthetic DNA system for structure-function studies of the high affinity CO2 uptake NDH-13 protein complex in cyanobacteria. Biochim Biophys Acta—Bioenerg. 2018; 1859: 1108–1118. https://doi.org/10.1016/j.bbabio.2018.06.015 PMID: 29959914

60. Deng Y, Ye J, Mi H. Effects of low CO2 on NAD(P)H dehydrogenase, a mediator of cyclic electron transport around photosystem I in the cyanobacterium *Synechocystis* PCC6803. Plant Cell Physiol. 2003; 44: 534–540. https://doi.org/10.1093/pcp/pcg067 PMID: 12773640

61. Xu M, Lv J, Fu P, Mi H. Oscillation kinetics of post-illumination increase in Chl fluorescence in cyanobacterium *Synechocystis* PCC 6803. 2016; 7: 1–7. https://doi.org/10.3389/fpls.2016.00108 PMID: 26913039

62. Xiong J, Hutchison RS, Sayre RT, Govindjee. Modification of the photosystem II acceptor side function in a D1 mutant (arginine-269-glycine) of *Chlamydomonas reinhardti*. Biochim Biophys Acta—Bioenerg. 1997; 1322: 60–76. https://doi.org/10.1016/S0005-2728(97)00063-7

63. Robinson HH, Eaton-Rye JJ, Van Rensen JJS, Govindjee. The effects of bicarbonate depletion and formate incubation on the kinetics of oxidation-reduction reactions of the Photosystem II Quinone Acceptor Complex. Zeitschrift für Naturforsch C. 1984; 39: 382–385. https://doi.org/10.1515/znc-1984-0514

64. Stirbet A, Riznichenko GY, Rubin AB, Govindjee. Modeling chlorophyll a fluorescence transient: Relation to photosynthesis. Biochem (Moscow). 2014; 79: 291–323. https://doi.org/10.1134/S0006297914040014 PMID: 24910205

65. Stirbet A, Lazár D, Kromdijk J, Govindjee. Chlorophyll a fluorescence induction: Can just a one-second measurement be used to quantify abiotic stress responses? Photosynthetica. 2018; 56: 86–104. https://doi.org/10.1007/s11099-018-0770-3

66. Schansker G, Tóth SZ, Strasser RJ. Methylviologen and dibromothymoquinone treatments of pea leaves reveal the role of photosystem I in the Chl a fluorescence rise OJIP. Biochim Biophys Acta—Bioenerg. 2005; 1706: 250–261. https://doi.org/10.1016/j.bbabio.2004.11.006 PMID: 15694353

67. Tsimilli-Michael M. Revisiting JIP-test: An educative review on concepts, assumptions, approximations, definitions and terminology. Photosynthetica. 2020; 58: 275–292. https://doi.org/10.32615/ps.2019.150

68. Bernát G, Appel J, Ogawa T, Rögner M. Distinct roles of multiple NDH-1 complexes in the cyanobacterial electron transport network as revealed by kinetic analysis of P700+ reduction in various ndh-deficient mutants of *Synechocystis* sp. strain PCC6803. J Bacteriol. 2011; 193: 292–295. https://doi.org/10.1128/JB.00984-10 PMID: 21036997

69. Cournac L, Mus F, Bernard L, Guedeney G, Vignais P, Peltier G. Limiting steps of hydrogen production in *Chlamydomonas reinhardtii* and *Synechocystis* PCC 6803 as analysed by light-induced gas exchange transients. Int J Hydrogen Energy. 2002; 27: 1229–1237. https://doi.org/10.1016/S0360-3199(02)00105-2

70. Ohkawa H, Pakrasi HB, Ogawa T. Two types of functionally distinct NAD(P)H dehydrogenases in *Synechocystis* sp. strain PCC6803. J Biol Chem. 2000; 275: 31630–31634. https://doi.org/10.1074/jbc.M003706200 PMID: 10906128

71. Battchikova N, Eisenhut M, Aro EM. Cyanobacterial NDH-1 complexes: Novel insights and remaining puzzles. Biochim Biophys Acta—Bioenerg. 2011; 1807: 935–944. https://doi.org/10.1016/j.bbabio.2010.10.017 PMID: 21035426

72. Zhao J, Gao F, Fan DY, Chow WS, Ma W. NDH-1 is important for photosystem I function of *Synechocystis* sp. Strain PCC 6803 under environmental stress conditions. Front Plant Sci. 2018; 8: 1–10. https://doi.org/10.3389/fpls.2017.02183 PMID: 29387069

73. Müller S, Zavřel T, Červený J. Towards a quantitative assessment of inorganic carbon cycling in photosynthetic microorganisms. Eng Life Sci. 2019; 19: 955–967. https://doi.org/10.1002/elsc.201900061 PMID: 32624985